International Journal of Solids and Structures 48 (2011) 1962–1990

Contents lists available at ScienceDirect

International Journal of Solids and Structures

journal homepage: www.elsevier.com/locate/ijsolstr

Gradient elasticity in statics and dynamics: An overview of formulations, length scale identification procedures, finite element implementations and new results

Harm Askes [a,*], Elias C. Aifantis [b]

[a] University of Sheffield, Department of Civil and Structural Engineering, Sheffield S1 3JD, United Kingdom
[b] Aristotle University of Thessaloniki, Polytechnic School, Laboratory of Mechanics and Materials, 54006 Thessaloniki, Greece

ARTICLE INFO

Article history:
Received 18 October 2010
Received in revised form 31 January 2011
Available online 15 March 2011

Keywords:
Gradient elasticity
Generalised continuum
Internal length scale
Wave dispersion
Singularity removal
Size effect

ABSTRACT

In this paper, we discuss various formats of gradient elasticity and their performance in static and dynamic applications. Gradient elasticity theories provide extensions of the classical equations of elasticity with additional higher-order spatial derivatives of strains, stresses and/or accelerations. We focus on the versatile class of gradient elasticity theories whereby the higher-order terms are the Laplacian of the corresponding lower-order terms. One of the challenges of formulating gradient elasticity theories is to keep the number of additional constitutive parameters to a minimum. We start with discussing the general Mindlin theory, that in its most general form has 903 constitutive elastic parameters but which were reduced by Mindlin to three independent material length scales. Further simplifications are often possible. In particular, the Aifantis theory has only one additional parameter in statics and opens up a whole new field of analytical and numerical solution procedures. We also address how this can be extended to dynamics. An overview of length scale identification and quantification procedures is given. Finite element implementations of the most commonly used versions of gradient elasticity are discussed together with the variationally consistent boundary conditions. Details are provided for particular formats of gradient elasticity that can be implemented with simple, linear finite element shape functions. New numerical results show the removal of singularities in statics and dynamics, as well as the size-dependent mechanical response predicted by gradient elasticity.

1. Introduction

Classical continuum solid mechanics theories, such as linear or nonlinear elasticity and plasticity, have been used in a wide range of fundamental problems and applications in civil, chemical, electrical, geological, mechanical and materials engineering, as well as in various fields of physics and life sciences. Even though the scales that these theories were initially designed for were ranging roughly from millimetre to metre, to describe deformation phenomena and processes that could be captured by the naked eye, they were also used in the last century to describe phenomena evolving at atomistic scales (elastic theory of dislocations), earth scales (faults and earthquakes) and astronomic scales (relativistic elastic solids). More recently, observations in advanced optical and electron microscopes have been interpreted by using classical continuum mechanics theory; in the last few years standard elasticity formulae have also been used to characterise deformation behaviour at the nanoscale (e.g. nanotubes or other nanoscale objects).

It is in this regime of micron and nano-scales that experimental evidence and observations with newly developed probes such as nano-indenters and atomic force microscopes have suggested that classical continuum theories do not suffice for an accurate and detailed description of corresponding deformation phenomena. More notably size effects could not be captured by standard elasticity and plasticity theories, even though such effects become dominant as the specimen or component size decreases. Moreover, classical elastic singularities as those emerging during the application of point loads or occurring at dislocation lines and crack tips cannot be removed, and the same is true for discontinuities occurring at interfaces. Another important class of problems that could not be treated with classical theory is when the homogeneous stress–strain curve contains a negative slope regime where strain softening or a phase transformation occurs. This is the case with elastic (twinning, martensitic transformations) and plastic (necking, shear banding) instabilities where classical theory could not provide any information on their evolution and spatio-temporal characteristics.

* Corresponding author. Tel.: +44 114 2225769; fax: +44 114 2225700.
E-mail address: h.askes@sheffield.ac.uk (H. Askes).

0020-7683/$ - see front matter © 2011 Elsevier Ltd. All rights reserved.
doi:10.1016/j.ijsolstr.2011.03.006

1.1. Enriched continuum theories in solid mechanics

Roughly speaking, the inability of standard continuum mechanics theories to deal with the above problems is due to the absence of an internal length, characteristic of the underlying microstructure, from the constitutive equations. Special materials science models and related atomistic or molecular simulations were used extensively as an alternative, but a convenient and sufficiently general mechanism-insensitive framework was lacking. On the other hand, a plethora of articles on generalised continuum mechanics appeared in the 1960s along the lines set out by the brothers Cosserat in the early 1900s (micropolar, micromorphic). However, they were excessively complex with too many parameters and equations to convince the experimentalist and motivate the designer to consider them seriously. Even more importantly, the majority of these theories were useful for dispersive wave propagation studies only, and key issues on non-convex equations of state and associated material instabilities along with size effects were not touched upon. A brief but self-contained review on generalised continuum mechanics theories as related to the present article can be found in Altan and Aifantis (1997).

It was only in the 1980s that Aifantis proposed a simple model of gradient plasticity for strain softening materials, motivated by gradient dislocation dynamics, in order to determine the width of shear bands (Aifantis, 1984, 1987). The simplicity of this formulation relies in the fact that only one additional constitutive constant is required. The resulting model also dispenses with non-uniqueness and non-convergence of mesh-size dependent finite element simulations. This was readily shown by de Borst and Mühlhaus (1992), de Borst et al. (1995) as well as Tomita and Fujimoto (1995) who used the shear band solution of Aifantis as a benchmark for their gradient code development. This strand of work has been extended by various other authors to damage problems later on in the 1990s (Fremond and Nedjar, 1996; Peerlings et al., 1996a; Comi, 1999).

In the beginning of the 1990s, Aifantis proposed another simple model with only one additional constant for use in elasticity (Aifantis, 1992). This gradient elasticity model has been shown to eliminate strain singularities from dislocation lines and crack tips (Altan and Aifantis, 1992; Ru and Aifantis, 1993). Even though this model could be formally obtained as a special case of the earlier gradient elasticity theories of the 1960s, its physical motivation originated from elastic considerations of nano-polycrystals and its specific form could not be guessed or concluded by formal considerations alone. This model revived the interest in gradient elasticity and a large number of papers have been published in the last two decades on this topic. Several issues related to the form and sign of the gradient terms and associated gradient coefficients, the corresponding extra boundary conditions and their physical meaning, the elimination of elastic singularities and the prediction of size effects, as well as numerical aspects and experimental validation, are still open and need further consideration. It is indeed the aim of this paper to provide a critical review of the above aspects and to present some fresh perspectives and new results.

1.2. Historical overview of gradient elasticity

The use of gradient elasticity to simulate the mechanical behaviour of materials and structures is not a novel idea – in fact, it has been advocated for more than a century and a half. However, the scope of study has varied widely over the years. This has already been touched upon in the previous Section, but in this Section we will provide a more systematic discussion focussed on elasticity that will also help in providing perspective to the remainder of the paper. We will distinguish three main periods of activity, each of which has its own focus.[1]

1.2.1. Pioneers

There have been some sporadic efforts in the 19th century to enrich the continuum equations of elasticity with additional higher-order derivatives so as to capture the effects of microstructure. As early as the 1850s, Cauchy suggested the use of higher-order spatial derivatives in the continuum equations in order to approximate the behaviour of discrete lattice models with more accuracy, whereby the size of the elementary volume appeared as an additional constitutive parameter (Cauchy, 1850a,b, 1851). These initial efforts were of an explorative character; they were not aimed at mathematical completeness but instead at capturing certain physical phenomena.

Somewhat later, Voigt developed a comprehensive description of the kinematics, balance laws and constitutive relations of discrete lattice models for crystals. He included molecular rotations alongside molecular displacements, as well as their conjugated forces (Voigt, 1887a). However, the resulting differential equations were quite complicated and solutions of boundary value problems were found only by making a number of additional assumptions (Voigt, 1887b,c). In the early 20th century, this area of research was expanded through the work of the Cosserat brothers. They equipped the kinematics of the three-dimensional continuum equations with three displacement components as well as three micro-rotations and included the couple-stresses, which are conjugated to the micro-rotations, in the equations of motion (Cosserat and Cosserat, 1909).

1.2.2. Renaissance

Despite some isolated activities in the first half of the 20th century, it was not until the 1960s that a major revival took place. Interestingly, this occurred around the same time on either side of the then East–West divide. Landmark papers of the Soviet school include Aero and Kuvshinskii (1961), Pal'mov (1964), Kunin (1966) and Vdovin and Kunin (1966); see also the somewhat later work of Levin (1971). From the Western school, the most renowned papers are those by Toupin (1962, 1964), Mindlin and Tiersten (1962), Mindlin (1964, 1965, 1968), Mindlin and Eshel (1968), Kröner (1963, 1967) and Green and Rivlin (1964a,b).

Initially, the focus of these studies was on extension of the Cosserat theory and couple-stress theories (Toupin, 1962; Mindlin and Tiersten, 1962; Toupin, 1964), but these were also extended into elaborate full gradient theories (Kröner, 1963; Green and Rivlin, 1964a; Mindlin, 1964, 1965; Mindlin and Eshel, 1968). Many of the latter studies are quite complicated theories aimed at generating and including a mathematically complete set of higher-order gradients, rather than focussing at a more limited set of higher-order gradients that are essential to capture the physical phenomena of interest.

1.2.3. Modern times

A second revival took place in the 1980s and beyond. Eringen derived a simple stress-gradient theory from his earlier integral nonlocal theories (Eringen, 1983), although interest in this work has remained largely dormant till the late 1990s. On the other

[1] Incidentally, there is a remarkable similarity between the history of gradient elasticity and the history of Greece, going from Ancient Greece as the cradle of European civilisation, via the baroque splendour of the Byzantine Empire, to the renewed vigour and focus of Modern Greece – with periods of relative silence in between (Özkirimli and Sofos, 2008). This analogy may serve as a tribute to the many members of the Greek mechanics community who have contributed to the development of gradient elasticity theories, in particular Professor Ioannis Vardoulakis (*1949–†2009), a close collaborator of the second author in the initial stages of the third wave of gradient theory development.

hand, inspired by earlier studies in plasticity (Aifantis, 1984, 1987) Aifantis and coworkers formulated gradient elasticity theories for finite deformations (Triantafyllidis and Aifantis, 1986) and infinitesimal deformations (Aifantis, 1992; Altan and Aifantis, 1992; Ru and Aifantis, 1993). Subsequently, these theories were extended with additional terms accounting for surface effects (Vardoulakis et al., 1996; Exadaktylos et al., 1996). Compared to the more elaborate theories of the 1960s, these newer theories are much simpler in that they contain fewer higher-order terms, which is manifested by the smaller number of additional constitutive constants that need experimental validation. Indeed, the guiding principle in formulating these theories has been to include only those higher-order terms that are required to describe the pertinent physics (such as localisation of strain without singularities). Similarly, in dynamics the focus was on formulating simple theories with as few additional constitutive coefficients as possible and to relate these coefficients to lattice geometries – see Andrianov et al. (2003, 2010b) for recent reviews.

With the increase of using computer methods for simulations, the implementation of gradient elasticity became the focus of a few studies. Especially *finite element* implementations of gradient elasticity tend to be non-trivial due to the more complex structure of the governing partial differential equations. Whilst certain authors have focussed on implementing the more complete (and more complicated) theories of the 1960s, see for instance (Shu et al., 1999; Amanatidou and Aravas, 2002; Zervos, 2008; Papanicolopulos et al., 2009), some others have exploited the simplicity offered by the Aifantis theory which has led to notably straightforward finite element implementations (Tenek and Aifantis, 2002; Askes et al., 2008b; Askes and Gitman, 2009).

1.3. A note on methodology: complexity versus simplicity

In formulating models for engineering science, a balance must be found between induction (deriving general principles from particular cases) and deduction (deriving particular cases from general principles). More particularly, engineering science requires experimental validation as well as theoretical development. Whilst the main focus here is not on experimental validation of gradient theories, we wish to emphasize that models in general, and gradient theories in particular, should not be more complicated than is warranted by experimental observations. Pleas for simplicity have been made throughout history, for instance:

> "we may assume the superiority, other things remaining equal, of the demonstration which derives from fewer postulates or hypotheses",

as attributed to Aristotle. Isaac Newton noted as his first of four rules of reasoning in philosophy that

> "nature is pleased with simplicity, and affects not the pomp of superfluous causes",

whereas more recently Albert Einstein opined that

> "[a]ny fool can make things bigger, more complex, and more violent. It takes a touch of genius – and a lot of courage – to move in the opposite direction."

We will apply this methodological principle of striving for simplicity in discussing gradient elasticity theories, especially concerning the number of additional parameters in a theory.

1.4. Aim, objectives and outline

In this paper, we set out to clarify a number of aspects of gradient elasticity that are sometimes deemed controversial or unresolved. Thus, we will discuss various formats of gradient elasticity and how they are related to each other. We will also treat the use of gradient elasticity in statics versus its use in dynamics, the identification of the additional constitutive constants, finite element implementations and appropriate formats of the boundary conditions.

We will start the paper with an overview of various gradient elasticity theories in Section 2, with particular emphasis on those theories whereby the higher-order terms can be written as the Laplacian of associated lower-order terms. Thus, we treat the theories of Mindlin, Eringen and Aifantis, as well as pertinent extensions to dynamics. Some gradient elasticity formulations used in dynamics turn out to be unstable, and in Section 3 we will review two studies from the recent literature where such formulations are used, with suggestions for improvement. Next, the identification and quantification of the length scale parameters is treated in Section 4. We provide an overview of various studies whereby the length scales are related to the size of the corresponding Representative Volume Elements or other microstructural properties via analytical, numerical or experimental techniques. The finite element implementation of gradient elasticity is discussed in Section 5. Whilst this is generally not a trivial task, we show that the theory of Aifantis and its extension to dynamics allow for simple and straightforward finite element implementations.

Whereas Section 2 gives an overview of the various theories available in the literature and Sections 3–5 provide discussions of earlier results, Section 6 presents original results that demonstrate the capability of gradient elasticity to avoid singularities in the stress and strain fields as well as the capability to predict size-dependent mechanical response. Some concluding remarks are given in Section 7.

2. Overview of various gradient elasticity formats

Many different formats of elasticity theories with microstructural influences exist. For instance, one could distinguish *mono-scale* formulations, in which all variables are defined on a single scale of observation, and *multi-scale* formulations, where different variables relate to different scales of observation. One could also distinguish between the nature of the additional variables, which may or may not aim to describe internal rotations of the medium – internal rotations are included in so-called Cosserat-type theories, couple stress theories and micropolar theories.

We will not attempt to provide a complete overview of all types of elasticity theories with microstructural effects. Thus, we will not consider Cosserat-type or micropolar theories, and we will focus on linear elasticity theories with infinitesimal strains. We will start with a brief discussion of Mindlin's theory of elasticity with microstructure, which is multi-scale in that it incorporates kinematic quantities at macro-scale and micro-scale, but afterwards we will focus on mono-scale theories where gradient-enrichment takes the form of the Laplacian of the relevant state variables.

2.1. Mindlin's 1964 theory

In a landmark paper, Mindlin (1964) presented a theory of elasticity with microstructure. He distinguished between kinematic quantities on the microscale and on the macroscale, and the kinetic energy density $\mathcal{T}$ as well as the deformation energy density $\mathcal{U}$ were written in terms of quantities at both scales. In particular,

$$\mathcal{T} = \frac{1}{2}\rho\dot{u}_i\dot{u}_i + \frac{1}{2}\rho\ell_1^2\dot{\psi}_{ij}\dot{\psi}_{ij} \tag{1}$$

and

$$\mathcal{U} = \frac{1}{2}C_{ijkl}\varepsilon_{ij}\varepsilon_{kl} + \frac{1}{2}B_{ijkl}\gamma_{ij}\gamma_{kl} + \frac{1}{2}A_{ijklmn}\kappa_{ijk}\kappa_{lmn} + D_{ijklm}\gamma_{ij}\kappa_{klm} + F_{ijklm}\kappa_{ijk}\varepsilon_{lm} + G_{ijkl}\gamma_{ij}\varepsilon_{kl} \tag{2}$$

where u_i, ε_{ij}, ψ_{ij}, γ_{ij} and κ_{ijk} are the macroscopic displacement, the macroscopic strain, the microscopic deformation, the relative deformation (i.e. the difference between macroscopic and microscopic deformation) and the gradient of the microscopic deformation, respectively. As such, we have $\varepsilon_{ij} = \frac{1}{2}(u_{i,j} + u_{j,i})$, $\gamma_{ij} = u_{j,i} - \psi_{ij}$ and $\kappa_{ijk} = \psi_{jk,i}$. Furthermore, ρ is the mass density (assumed to be equal at both scales of observation) and ℓ_1 is related to the size of the unit cell of the microstructure. Finally, the constitutive tensors C_{ijkl}, B_{ijkl}, A_{ijklmn}, D_{ijklm}, F_{ijklm} and G_{ijkl} contain 1764 coefficients, a daunting 903 of which are independent (Mindlin, 1964). For isotropic materials, the number of independent elastic constitutive coeffients reduces to a much more tractable, yet still considerable, amount of 18, by which the deformation energy density of Eq. (2) can be written as (Mindlin, 1964)

$$\begin{aligned}\mathcal{U} = {} & \frac{1}{2}\lambda\varepsilon_{ii}\varepsilon_{jj} + \mu\varepsilon_{ij}\varepsilon_{ij} + \frac{1}{2}b_1\gamma_{ii}\gamma_{jj} + \frac{1}{2}b_2\gamma_{ij}\gamma_{ij} + \frac{1}{2}b_3\gamma_{ij}\gamma_{ji} + g_1\gamma_{ii}\varepsilon_{jj} \\ & + g_2\left(\gamma_{ij} + \gamma_{ji}\right)\varepsilon_{ij} + a_1\kappa_{iik}\kappa_{kjj} + a_2\kappa_{iik}\kappa_{jkj} + \frac{1}{2}a_3\kappa_{iik}\kappa_{jjk} \\ & + \frac{1}{2}a_4\kappa_{ijj}\kappa_{ikk} + a_5\kappa_{ijj}\kappa_{kik} + \frac{1}{2}a_8\kappa_{iji}\kappa_{kjk} + \frac{1}{2}a_{10}\kappa_{ijk}\kappa_{ijk} \\ & + a_{11}\kappa_{ijk}\kappa_{jki} + \frac{1}{2}a_{13}\kappa_{ijk}\kappa_{ikj} + \frac{1}{2}a_{14}\kappa_{ijk}\kappa_{jik} + \frac{1}{2}a_{15}\kappa_{ijk}\kappa_{kji}\end{aligned} \tag{3}$$

where λ and μ are the usual Lamé constants and the various a_i, b_i and g_i are 16 additional constitutive coefficients.

The theoretical basis, completeness and richness of Mindlin's theory of elasticity with microstructure cannot be overstated. Yet, it must also be acknowledged that for practical purposes the use Eq. (3) is limited as it requires the formidable task of quantifying, experimentally or otherwise, the 16 additional coefficients. However, Mindlin also formulated simpler versions of his elasticity theory with microstructure, in which a number of assumptions are made that allow to express the deformation energy density in terms of the macroscopic displacements u_i only, thus dropping the multi-scale character of Eqs. (1)–(3). These were denoted as Forms I, II and III, respectively, and they differ in the assumed relation between the microscopic deformation gradient κ_{ijk} and the macroscopic displacement u_i.

- Form I: The microscopic deformation gradient is defined as the second gradient of the macroscopic displacement: $\kappa_{ijk} = u_{k,ij}$.
- Form II: The microscopic deformation gradient is assumed to be the first gradient of the macroscopic strain, that is $\kappa_{ijk} = \varepsilon_{jk,i}$ and in turn $\kappa_{ijk} = \frac{1}{2}(u_{k,ij} + u_{j,ik})$.
- Form III: The last form is slightly different in that it splits the microscopic deformation effects into two parts, namely a gradient of macroscopic rotation $\chi_{ij} = \frac{1}{2}e_{jlm}u_{m,il}$ (where e_{jlm} is the Levi–Civita permutation tensor) and the symmetric part of the second gradient of macroscopic displacement $\kappa_{ijk} = \frac{1}{3}(u_{i,jk} + u_{j,ik} + u_{k,ij})$.

Nevertheless, despite the theoretical differences between the three forms, the equations of motion of the three forms are identical, whether expressed in terms of displacements (Mindlin, 1964) or in terms of stresses (Mindlin and Eshel, 1968). Since we wish to focus on the final format of the equations of motion, we will ignore the differences between the three Forms and concentrate on Form II for further derivations. The deformation energy density for Form II simplifies as

$$\begin{aligned}\mathcal{U} = {} & \frac{1}{2}\lambda\varepsilon_{ii}\varepsilon_{jj} + \mu\varepsilon_{ij}\varepsilon_{ij} + a_1\varepsilon_{ik,i}\varepsilon_{jj,k} + a_2\varepsilon_{jj,i}\varepsilon_{kk,i} + a_3\varepsilon_{ik,i}\varepsilon_{jk,j} \\ & + a_4\varepsilon_{jk,i}\varepsilon_{jk,i} + a_5\varepsilon_{jk,i}\varepsilon_{ij,k}\end{aligned} \tag{4}$$

where the definition of the various constitutive coefficients is slightly different from those in Eq. (3), but we will ignore this difference here – the interested reader is referred to Mindlin (1964). Although less well-known, Mindlin also suggested a simplification of the kinetic energy (Mindlin, 1964, Section 10), that is

$$\mathcal{T} = \frac{1}{2}\rho\dot{u}_i\dot{u}_i + \frac{1}{2}\rho\ell_1^2\dot{u}_{i,j}\dot{u}_{i,j} \tag{5}$$

With both these amendments to the kinetic and deformation energy densities, the equations of motion can be expressed entirely in terms of the macroscopic displacements as

$$\begin{aligned}(\lambda+\mu)u_{j,ij} + \mu u_{i,jj} - \frac{4a_1 + 4a_2 + 3a_3 + 2a_4 + 3a_5}{2}u_{j,ijkk} \\ - \frac{a_3 + 2a_4 + a_5}{2}u_{i,jjkk} + b_i = \rho(\ddot{u}_i - \ell_1^2\ddot{u}_{i,jj})\end{aligned} \tag{6}$$

where b_i are the body forces.

Although Eq. (6) still contains one additional inertia parameter (namely ℓ_1) as well as five additional elastic parameters (namely a_1–a_5), it can also be seen that the latter appear in two groups. Within the spirit of Section 1.3, the distinction between the various a_i is irrelevant for practical purposes. For this reason, we will write Eq. (6) as

$$(\lambda+\mu)\left(1 - \ell_2^2\frac{\partial^2}{\partial x_k^2}\right)u_{j,ij} + \mu\left(1 - \ell_3^2\frac{\partial^2}{\partial x_k^2}\right)u_{i,jj} + b_i = \rho\left(1 - \ell_1^2\frac{\partial^2}{\partial x_j^2}\right)\ddot{u}_i \tag{7}$$

where

$$\ell_2 = \sqrt{\frac{4a_1 + 4a_2 + 3a_3 + 2a_4 + 3a_5}{2(\lambda+\mu)}} \quad \text{and} \quad \ell_3 = \sqrt{\frac{a_3 + 2a_4 + a_5}{2\mu}} \tag{8}$$

so that now only three additional parameters appear, namely ℓ_1, ℓ_2 and ℓ_3. From Eq. (7) we can make a few pertinent observations. Firstly, the additional parameters ℓ_1, ℓ_2 and ℓ_3 have the dimension of length, and can be linked to the underlying microstructure, as we will explore further in Section 4. Secondly, all higher-order terms in the equations of motion are found as the Laplacian of the corresponding lower-order terms; this holds for the stiffness terms as well as for the inertia terms.

As we will see in Section 4, Laplacian-type gradients often appear naturally in microstructural motivations of gradient theories. There is also a strong physical background of Laplacian-type gradients, since Laplace operators describe diffusion processes and Laplacian-type gradients are thus representative for nonlocal redistribution effects. Thus, the most versatile gradients are, arguably, Laplacian-type gradients. In the remainder of this study we will concentrate on gradient elasticity theories that incorporate the Laplacian of relevant state variables. We will discuss these theories separately for use in statics and dynamics.

2.2. Laplacian-based theories for statics

The primary motivation for using gradient elasticity in statics has been to dispense with the singularities that appear at crack tips and dislocation cores. It has been shown on many occasions that these singularities can be avoided with an appropriate use of gradient elasticity (Eringen, 1983; Altan and Aifantis, 1992; Ru and Aifantis, 1993; Unger and Aifantis, 1995; Gutkin and Aifantis, 1996, 1997, 1999; Gutkin, 2000; Askes and Gutiérrez, 2006; Askes et al., 2008b). One of the most popular theories of gradient

elasticity is due to Aifantis and coworkers in the early 1990s (Aifantis, 1992; Altan and Aifantis, 1992; Ru and Aifantis, 1993). Although its formulation was inspired by earlier studies in gradient plasticity, not elasticity with microstructure, it was later demonstrated (Altan and Aifantis, 1997) that the Aifantis theory is formally a special case of the Mindlin theory as given in Eq. (7). Namely, the two length scales ℓ_2 and ℓ_3 of the Mindlin theory are in the Aifantis theory taken *equal* to each other, which greatly simplifies further mathematical and implementational treatment.

The Aifantis theory can be written in a number of alternative formats, and one of these formats exhibits stress gradients. Stress gradients also appear in an earlier yet less well-known theory of gradient elasticity, namely the one due to Eringen (1983). We will treat these two theories in chronological order. We will also clarify the differences between the Eringen theory and the Aifantis theory with stress gradients.

2.2.1. Eringen's 1983 theory

Eringen's work is probably best known for advocating the use of integral-type nonlocality, where volume averages of state variables are computed. For the purpose of the present discussion, we focus on nonlocal stresses. The nonlocal stress tensor, denoted as σ_{ij}^g, is computed from the local stress tensor, indicated with σ_{ij}^c, via

$$\sigma_{ij}^g(\mathbf{x}) = \int_V \alpha(\mathbf{s})\sigma_{ij}^c(\mathbf{x}+\mathbf{s})\mathrm{d}V \tag{9}$$

where the local stresses are related to the displacement gradients as usual, that is $\sigma_{ij}^c = C_{ijkl}u_{k,l}$. Furthermore, $\alpha(\mathbf{s})$ is a nonlocal weight function that is non-negative and decreasing for increasing values of $\mathbf{s}$. The meaning of Eq. (9) is that the nonlocal stress at point $\mathbf{x}$ is the weighted average of the local stress of all points in the neighbourhood of $\mathbf{x}$, the size of which is set via the definition of α.

Eringen also formulated a theory of nonlocal elasticity where the integrals are replaced by gradients (Eringen, 1983). The mathematical manipulations and the approximation error in going from integral-type nonlocality to gradient-type nonlocality depend on the choice of the weight function α, but the final result is given as a partial differential equation as

$$\sigma_{ij}^g - \ell^2\sigma_{ij,kk}^g = \sigma_{ij}^c = C_{ijkl}u_{k,l} \tag{10}$$

where ℓ is a length scale parameter, the magnitude of which follows from the definition of the nonlocal weight function α.

2.2.2. Aifantis' 1992 theory

In the early 1990s, motivated by earlier work in plasticity (Aifantis, 1984, 1987) and nonlinear elasticity (Triantafyllidis and Aifantis, 1986), Aifantis and coworkers suggested to extend the linear elastic constitutive relations with the Laplacian of the strain as (Aifantis, 1992; Altan and Aifantis, 1992; Ru and Aifantis, 1993)

$$\sigma_{ij} = C_{ijkl}\left(\varepsilon_{kl} - \ell^2\varepsilon_{kl,mm}\right) \tag{11}$$

where ℓ is again a length scale parameter. The associated equilibrium equations are

$$C_{ijkl}\left(u_{k,jl} - \ell^2 u_{k,jlmm}\right) + b_i = 0 \tag{12}$$

For isotropic linear elasticity, $C_{ijkl} = \lambda\delta_{ij}\,\delta_{kl} + \mu\delta_{ik}\delta_{jl} + \mu\delta_{il}\delta_{jk}$, and it is then easily verified that Eq. (12) is a special case of Eq. (7), namely with $\ell_2 = \ell_3 \equiv \ell$. It is also possible to derive Eq. (12) directly from Eq. (7) by requiring additional symmetries in the elastic energy of Eq. (4) as has been argued by Lazar and Maugin (2005).

In a follow-up work, Ru and Aifantis (1993) developed an *operator split* by which the fourth-order equilibrium Eq. (12) can be solved as an uncoupled sequence of two sets of second-order equations, that is

$$C_{ijkl}u_{k,jl}^c + b_i = 0 \tag{13}$$

followed by

$$u_k^g - \ell^2 u_{k,mm}^g = u_k^c \tag{14}$$

where two separate displacement fields are distinguished. Firstly, u_i^c obey the equations of classical elasticity (13) and therefore carry a superscript c. Secondly, u_i^g are the same as u_i in Eq. (12) but are appended a superscript g to emphasize that they are affected by the gradient activity as per Eq. (14). This operator split has also been used by Lurie et al. (2003).

When Eq. (14) is substituted into Eq. (13), the original Eq. (12) are retrieved, and with appropriate boundary conditions the solution of Eqs. (13) and (14) is the same as the solution of the original Eq. (12). However, the appeal of Eqs. (13) and (14) is their uncoupled format, which allows to solve u_i^c first from Eq. (13), after which u_i^g can be solved from Eq. (14). Such an approach greatly facilitates analytical and numerical solution strategies and is not possible with Mindlin's general gradient elasticity as given in Eq. (7).

Remark 1. Infinitely many simplifications of the general Mindlin gradient elasticity theory are possible by taking various ratios ℓ_2/ℓ_3. However, only the case $\ell_2 = \ell_3$ allows to replace Eq. (12) by Eqs. (13) and (14). Although the Aifantis theory is sometimes referred to as merely a simplification of the Mindlin theory, this particular simplification opens up a whole new field of solution methods that are not available for the Mindlin theory (or indeed other simplifications of the Mindlin theory, that is by taking $\ell_2/\ell_3 \neq 1$). In fact, many authors who set out to use the general Mindlin theory make the appealing particularisation towards the Aifantis theory, see for instance (Amanatidou and Aravas, 2002; Polyzos et al., 2003; Tsepoura et al., 2003; Papargyri-Beskou et al., 2009), although this is not always acknowledged as such (Georgiadis, 2003; Karlis et al., 2007; Georgiadis and Anagnostou, 2008).

Remark 2. Aifantis also suggested another Laplacian-based theory of gradient elasticity, whereby the gradient effects only affect the volumetric strain, not the total strain (Aifantis, 1995). As a result of this restricted gradient dependence the Ru-Aifantis operator-split cannot be applied to this particular format, and we will not consider this particular variant of gradient elasticity further.

In the original Ru-Aifantis approach the gradient-enrichment is expressed in terms of displacements, as given in Eq. (14). By differentiation, it is also possible to evaluate the gradient-enrichment in terms of strains (Gutkin and Aifantis, 1997, 1999; Askes et al., 2008b), that is

$$\varepsilon_{kl}^g - \ell^2\varepsilon_{kl,mm}^g = \varepsilon_{kl}^c = \frac{1}{2}\left(u_{k,l}^c + u_{l,k}^c\right) \tag{15}$$

or, after pre-multiplication with the constitutive tensor C_{ijkl}, as

$$C_{ijkl}\left(\varepsilon_{kl}^g - \ell^2\varepsilon_{kl,mm}^g\right) = C_{ijkl}u_{k,l}^c \tag{16}$$

whereby $\varepsilon_{kl}^g = \frac{1}{2}\left(u_{k,l}^g + u_{l,k}^g\right)$. The use of either Eq. (14), Eq. (15) or Eq. (16) in conjunction with Eq. (13) does not impact on the general solution of the field equations, but the variationally consistent boundary conditions are different in the various cases, see Section 5.3 and (Askes et al., 2008b) for more details. It was also shown that the use of Eq. (14) does not necessarily remove the singularities from all strain components at the tips of sharp cracks, whereas all singularities were removed when using Eqs. (15) or (16), as demonstrated by Askes et al. (2008b) and Askes and Gitman (2009), respectively.

2.2.3. Comparison of the Eringen theory and the Aifantis theory

The left-hand-side of Eq. (16) can of course also be interpreted in terms of stresses as (Gutkin, 2000; Askes et al., 2008b)

$$\sigma_{ij}^g - \ell^2\sigma_{ij,mm}^g = C_{ijkl}u_{k,l}^c \tag{17}$$

The fact that Eqs. (10) and (17) describe the same gradient dependence raises the obvious question: to which extent does the stress-based operator split Aifantis theory coincide with the earlier Eringen theory?

The answer to this question lies in the format of the balance of momentum equations (Askes and Gitman, 2010). In Eringen's theory, equilibrium is expressed in terms of the divergence of σ^g_{ij}, whereas in Aifantis' theory the divergence of σ^c_{ij} is used, i.e.

$$\sigma^g_{ij,j} + b_i = 0 \quad \text{(Eringen)} \tag{18}$$

versus

$$\sigma^c_{ij,j} + b_i = 0 \quad \text{(Aifantis)} \tag{19}$$

In the Aifantis theory, σ^c_{ij} can be obtained directly from the derivative of the displacements u^c_i, therefore Eq. (19) can also be written as a set of n^{sd} equations with n^{sd} displacement unknowns u^c_i, where n^{sd} is the number of spatial dimensions. As mentioned above, these displacements u^c_i can then be used as input for Eq. (17), and the result is an *uncoupled* set of equations, namely Eq. (13) followed by Eq. (17). In contrast, in the Eringen theory the relation between the equilibrated stress tensor, which is σ^g_{ij}, and the displacements is a *differential equation* as given in Eq. (10). As a result, Eqs. (10) and (18) are *coupled* and must thus be solved simultaneously.

The implications for numerical implementations are significant, as will be discussed in Section 5. However, a unification of the two theories is also possible and will be addressed in Section 2.4.2.

2.3. Laplacian-based theories for dynamics

We will now focus our attention on Laplacian-based gradient elasticity theories for dynamics. The main motivation for using gradient elasticity in dynamics has been the description of dispersive wave propagation through heterogeneous media, rather than the removal of stress and/or strain singularities. Many researchers have derived gradient elasticity models from associated lattice models consisting of discrete masses and springs. The resulting models are often of the format of Eq. (11), although the sign of the higher-order term tends to be positive, not negative as in Eq. (11). Whereas the strain gradients with negative sign are stable, strain gradients with positive sign are destabilising, which has been demonstrated on various occasions, e.g. (Askes et al., 2002; Metrikine and Askes, 2002). The sign of the gradient term and the issues of uniquenss and stability versus the ability to describe dispersive wave propagation have led to a lot of discussion, see for instance the early study of Mindlin and Tiersten (1962) and more recently Yang and Guo (2005) or Maranganti and Sharma (2007) where this dilemma was called the "sign paradox". Comparative studies between the models with positive and negative sign were presented by Unger and Aifantis (2000a,b) and Askes et al. (2002).

However, with a few mathematical manipulations it is fairly straightforward to translate the unstable strain gradients into stable gradients of stress or acceleration. Such modifications of unstable gradients are the key to unifying gradient elasticity formulations for statics and dynamics (Askes and Aifantis, 2006).

2.3.1. Lattice dynamics and unstable strain gradients

In many studies, gradient elasticity theories have been derived from the continualisation of the response of a discrete lattice, see for instance an early work of Mindlin (1968) or more recently Chang and Gao (1995), Rubin et al. (1995), Mühlhaus and Oka (1996). To illustrate this approach, we will consider the one-dimensional chain of particles and springs depicted in Fig. 1. All particles have mass M and all springs have spring stiffness K; furthermore, the particle spacing is denoted with d. The equation of motion of the central particle n is written as

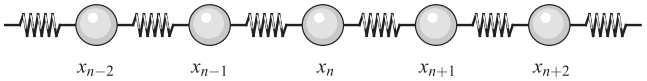

Fig. 1. One-dimensional discrete model consisting of particles and springs.

$$K(u_{n+1} - 2u_n + u_{n-1}) = M\ddot{u}_n \tag{20}$$

Continualisation is performed by translating the response of the discrete model into a continuous displacement field $u(x,t)$. For the central particle this implies $u_n(t) = u(x,t)$ and for the neighbouring particles $u_{n\pm1} = u(x \pm d, t)$. Taylor series are applied to the latter, that is

$$u(x \pm d, t) = u(x,t) \pm du(x,t)_{,x} + \frac{1}{2}d^2u(x,t)_{,xx} \pm \cdots \tag{21}$$

by which Eq. (20) can be rewritten as

$$E\left(u_{,xx} + \frac{1}{12}d^2u_{,xxxx} + \cdots\right) = \rho\ddot{u} \tag{22}$$

where the mass density $\rho = M/Ad$, the Young's modulus $E = Kd/A$ and A is the cross-sectional area. When terms of order d^4 and higher are ignored, the constitutive equation that can be retrieved from Eq. (22) reads

$$\sigma = E\left(\varepsilon + \frac{1}{12}d^2\varepsilon_{,xx}\right) \tag{23}$$

As can be verified, the main difference between Eqs. (23) and (11) concerns the sign of the strain gradient terms. The strain gradients in Eq. (11) are equivalent to those derived from the positive-definite deformation energy density of Eq. (4), and therefore the strain gradients in Eq. (11) are stable. By implication, the opposite sign of the strain gradient term in Eq. (23) makes this term *destabilising*. Instabilities manifest themselves in dynamics by an unbounded growth of the response in time without external work. Instabilities are also related to loss of uniqueness in static boundary value problems – see Askes et al. (2002) for a discussion and examples of instabilities in statics and dynamics.

Multi-dimensional extensions of Eq. (23) have been derived on many occasions. The exact format of the stress–strain relations depends on the types of particle interactions that are taken into account, but a general representation of such models can be written as (Chang and Gao, 1995; Mühlhaus and Oka, 1996; Suiker and de Borst, 2001; Askes and Metrikine, 2005; Vasiliev et al., 2010)

$$\sigma_{ij} = C_{ijkl}\left(\varepsilon_{kl} + \ell^2\varepsilon_{kl,mm}\right) \tag{24}$$

where the length scale parameter ℓ is usually a closed-form algebraic expression in terms of the particle spacing d. The positive sign that precedes the higher-order strain gradients in Eq. (24) again indicates that such terms are destabilising.

2.3.2. Stable stress gradients or stable acceleration gradients

Many researchers have realised the instability of the strain gradients given in Eqs. (23) and (24) and suggested modifications that avoid instabilities, e.g. Collins (1981), Rubin et al. (1995), Chen and Fish (2001), Andrianov et al. (2003), Andrianov and Awrejcewicz (2008), Pichugin et al. (2008), Andrianov et al. (2010b). One of the used techniques consists of taking the Laplacian of Eq. (24), multiplying with ℓ^2 and substracting the result from the original Eq. (24), by which

$$\sigma_{ij} - \ell^2\sigma_{ij} = C_{ijkl}\varepsilon_{kl} \tag{25}$$

where terms of order ℓ^4 have been ignored. Clearly, Eq. (25) is equivalent to Eq. (10). The energy functional underlying Eq. (25) is positive definite in terms of stresses and stress gradients, see

e.g. (Askes and Gutiérrez, 2006), hence the unstable strain gradients of Eq. (24) have been replaced by stable stress gradients.

The equations of motion based on Eq. (24) read

$$C_{ijkl}\left(u_{k,jl}+\ell^2 u_{k,jlmm}\right)+b_i=\rho\ddot{u}_i \tag{26}$$

The technique described in going from Eq. (24) to Eq. (25) can also be applied to Eq. (26), leading to

$$C_{ijkl}u_{k,jl}+b_i=\rho\left(\ddot{u}_i-\ell^2\ddot{u}_{i,mm}\right) \tag{27}$$

where the unstable strain gradients have now been replaced by acceleration gradients. Comparison of Eq. (27) with Eqs. (5) and (6) shows that the acceleration gradients of Eq. (27) are associated with a positive definite kinetic energy density and, therefore, they are stable.

Remark 3. Although at first sight the derivations of Eqs. (10) and (25) seem to be based on different arguments, one can derive Eq. (24) via a Taylor series expansion from Eq. (9), as has been demonstrated by Huerta and Pijaudier-Cabot (1994), Peerlings et al. (1996b).

Remark 4. Eq. (27) can also be derived from Eq. (25) by taking the Laplacian of the generic equations of motion $\sigma_{ij,j}+b_i=\rho\ddot{u}_i$, multiplying with ℓ^2 and substituting Eq. (25). Thus, Eqs. (25) and (27) are closely related. In infinite continua they produce the same dispersive behaviour of propagating waves, although the boundary conditions take different formats in the two models.

2.4. Dynamic consistency

The main motivation to use gradient elasticity in statics was to avoid singularities in the elastic fields, as explained in Section 2.2 – this can be achieved with stress gradients or with stable strain gradients. The main motivation for gradient elasticity in dynamics was to describe dispersive wave propagation, which can be done with unstable strain gradients, stress gradients or acceleration gradients, cf. Section 2.3. It is of interest to see which gradients, or which combinations of gradients, produce a theory that is applicable to statics as well as dynamics.

2.4.1. Stable strain gradients and stable acceleration gradients

Obviously, combining stable and unstable strain gradients is not fruitful, since one of the two strain gradients will dominate and the effect of the other strain gradient will be lost; moreover, the dominant strain gradients could be destabilising. Stress gradients are capable of removing singularities and of capturing wave dispersion. Furthermore, stress gradients such as those in Eq. (25) are stable. Another powerful gradient elasticity theory is obtained by combining stable strain gradients with acceleration gradients. Such a theory was already suggested by Mindlin, cf. Eq. (7), see also (Georgiadis et al., 2000). More recently, a theory with (stable) strain gradients and acceleration gradients was derived from a discrete lattice, and the simultaneous appearance of the two types of gradients was denoted *dynamic consistency* (Metrikine and Askes, 2002; Askes and Metrikine, 2002; Metrikine and Askes, 2006). Such a model was also derived from various micromechanical considerations by Engelbrecht et al. (2005) and Gitman et al. (2005). A recent overview of applications in continuum mechanics and structural mechanics can be found in Papargyri-Beskou et al. (2009).

A dynamically consistent model incorporates more than one length scale. The simplest version is to take $\ell_2=\ell_3$ in Eq. (7), by which

$$C_{ijkl}\left(u_{k,jl}-\ell_s^2 u_{k,jlmm}\right)+b_i=\rho\left(\ddot{u}_i-\ell_d^2\ddot{u}_{i,mm}\right) \tag{28}$$

where ℓ_s is the relevant length scale for statics and ℓ_d is the length scale that is added for use in dynamics. The two length scales can be related to the size of the Representative Volume Element in statics and dynamics (Gitman et al., 2005; Bennett et al., 2007).

Remark 5. The causality of this model, and other gradient elasticity models, has been studied by Metrikine (2006) and Askes et al. (2008a), whereby causality is understood in the sense of Einstein: in a causal model a signal should not be able to propagate faster than the speed of light. To ensure causality, it was shown that another term, proportional to a fourth-order time derivative, must be included in the formulation. However, for simplicity we will not follow that particular recommendation in the present study.

2.4.2. Unification of the theories of Eringen and Aifantis

In Section 2.2.3 we discussed the gradient elasticity theories of Eringen and Aifantis, and their differences, from a statics point of view. However, a dynamics point of view provides further insight and can in fact be used to unify the two theories (Askes and Gitman, 2010). To illustrate this, we start with revisiting the concept of implicit constitutive equations, applied to gradient elasticity. Implicit constitutive relations seem to have been pioneered by Morgan (1966) and have more recently been expanded by Rajagopal (2003, 2007). For the specific case of Laplacian-based gradient elasticity, a generic implicit constitutive equation can be written as

$$\left(1-g_1\frac{\partial^2}{\partial x_m^2}\right)\sigma_{ij}=C_{ijkl}\left(1-g_2\frac{\partial^2}{\partial x_m^2}\right)\varepsilon_{kl} \tag{29}$$

where g_1 and g_2 are two generic constitutive constants that can be expressed in terms of (the square of) the length scale parameter ℓ. Eq. (29) must, as always, be accompanied by balance of momentum and strain–displacement relations.

Firstly, we consider the static case. Expressing the equilibrium equations as $\sigma_{ij,j}+b_i=0$, it can be easily verified that Eringen's theory is obtained by setting $g_2=0$ and Aifantis' 1992 theory by taking $g_1=0$. The subsequent operator split formulations of Eqs. (14) and (15) can also be obtained via $\sigma_{ij,j}+b_i=0$ and $g_1=0$. Conversely, the stress-based formulation of Eq. (16) is obtained by setting $g_2=0$ but by expressing the equilibrium equations in terms of $C_{ijkl}\,\varepsilon_{kl}$ instead of σ_{ij}, as already commented upon in Section 2.2.3. Whereas Eq. (15) removes singularities from the strain field and Eq. (16) removes singularities from the stress field, the most general version of Eq. (29), that is taking $g_1\neq 0$ and $g_2\neq 0$, has recently been discussed by Aifantis (2003) and shown to be able to eliminate singularities from stress *and* strain fields.

For the dynamic case, we start with the usual equations of motion $\sigma_{ij,j}+b_i=\rho\ddot{u}_i$. In order to substitute the implicit constitutive relation (29), one can take the Laplacian of the equations of motion, multiply these with g_1, and substract the result from the original equations of motion. The result is

$$\left(1-g_1\frac{\partial^2}{\partial x_m^2}\right)\sigma_{ij,j}+b_i=\rho\left(\ddot{u}_i-g_1\ddot{u}_{i,mm}\right) \tag{30}$$

where it is assumed that the second derivatives of the body forces vanish. Substitution of Eq. (29) then yields

$$C_{ijkl}\left(1-g_2\frac{\partial^2}{\partial x_m^2}\right)\varepsilon_{kl,j}+b_i=\rho\left(\ddot{u}_i-g_1\ddot{u}_{i,mm}\right) \tag{31}$$

which is identical to the dynamically consistent gradient elasticity given in Eq. (28) for $g_1=\ell_d^2$ and $g_2=\ell_s^2$. Hence, in terms of *equations*

of motion, the dynamically consistent gradient elasticity model, which is a particular case of the Mindlin model, unifies the gradient elasticity theories of Eringen and Aifantis, whereby the acceleration gradients play the role of the gradients due to Eringen and the strain gradients are the same as those in the Aifantis theory.

In terms of *constitutive relations*, the implicit constitutive equation given in expression (29) provides a similar unification, as argued above, although this would then raise the obvious question how such an implicit constitutive equation for gradient elasticity could be motivated. As a partial answer to this question, the arguments of *scale invariance* in gradient elasticity outlined by Aifantis (2009b) could be exploited. The macroscopic stress tensor σ_{ij} and strain tensor ε_{ij} can be related to their atomic *scalar* counterparts s and e via (Aifantis, 2009b)

$$\sigma_{ij} = (a_\sigma \delta_{ij} + b_\sigma M_{ij}) s \quad \text{and} \quad \varepsilon_{ij} = (a_\varepsilon \delta_{ij} + b_\varepsilon M_{ij}) e \tag{32}$$

where the various a and b are upscaling constants. Furthermore, $M_{ij} = \frac{1}{2}(m_i n_j + m_j n_i)$ where m_i and n_i denote the orthonormal vectors that set the directions of the atomic lattice. The format of the (scalar) atomic stress–strain relation between s and e sets the format of the (tensorial) macroscopic stress–strain relation between σ_{ij} and ε_{ij}, as explained in Aifantis (2009b). Thus, using the classical relation $s = Ke$ on the atomic scale with K a constant, we obtain the classical relation $\sigma_{ij} = C_{ijkl}\varepsilon_{kl}$ on the macroscale. However, if the atomic scale stress–strain relation takes the implicit gradient format of $s - g_1 s_{,kk} = K(e - g_2 e_{,kk})$, then the macroscale stress-relation adopts the format given in Eq. (29). Thus, a tensorial macroscale implicit constitutive equation can be derived from a scalar atomic scale implicit constitutive equation. Whilst this does not provide a complete motivation for implicit constitutive equations, it should nevertheless be simpler to derive these in a scalar format than in a tensorial format. This is, however, left for future research.

2.5. Dispersion analysis

To assess the differences between the various formats of gradient elasticity discussed in the previous sections, and to assess their relevance for dynamic applications, the dispersive properties are studied next. For simplicity and transparency of argument, the one-dimensional case is investigated first, and some comments about the multi-dimensional case are made afterwards. Of the different models presented in Section 2.3 only two need to be distinguished, namely those of Eqs. (28) and (25) – the models of Eqs. (24) and (27) can be retrieved through a suitable parameter choice from the model of Eq. (28).

For completeness, we will also include the results of the Aifantis model given in Eq. (11), although this theory was proposed for use in statics rather than dynamics.

2.5.1. One-dimensional case

A general harmonic solution $u(x,t) = \hat{u}\exp(\mathrm{i}(kx - \omega t))$ is assumed, where $\hat{u}$ is the amplitude, i is the imaginary unit, k is the wave number and ω is the angular frequency. Substituting this solution into the one-dimensional version of Eq. (28) yields

$$\frac{\omega^2}{k^2 c_e^2} = \frac{1 + \ell_s^2 k^2}{1 + \ell_d^2 k^2} \tag{33}$$

where $c_e = \sqrt{E/\rho}$ is the elastic bar velocity and E the Young's modulus. The models of Eqs. (11) and (27) are found by taking $\ell_d = 0$ and $\ell_s = 0$, respectively. Furthermore, the model of Eq. (24) is found by taking $\ell_d = 0$ and by replacing ℓ_s^2 with $-\ell_s^2$.

For the model of Eq. (25), simultaneous solutions for the displacement $u(x,t) = \hat{u}\exp(\mathrm{i}(kx - \omega t))$ and the stress $\sigma(x,t) = \hat{\sigma}\exp(\mathrm{i}(kx - \omega t))$ are considered, where $\hat{\sigma}$ is the amplitude for the stress solution. With these substitutions, the equation of motion $\rho\ddot{u} = \sigma_{,x}$ gives

$$-\rho\omega^2\hat{u} = \mathrm{i}k\hat{\sigma} \tag{34}$$

and Eq. (25) itself yields

$$(1 + \ell^2 k^2)\hat{\sigma} = \mathrm{i}Ek\hat{u} \tag{35}$$

Elimination of $\hat{u}$ and $\hat{\sigma}$ then results in

$$\frac{\omega^2}{k^2 c_e^2} = \frac{1}{1 + \ell^2 k^2} \tag{36}$$

Note that the latter result is also obtained with the model of Eq. (27), cf. Eq. (33) with $\ell_s = 0$. Thus, for the description of one-dimensional wave dispersion the model with stress gradients and the model with acceleration gradients are equivalent.

In Fig. 2 the phase velocity $c = \omega/k$ (normalised with c_e) is plotted against the wave number k (normalised with ℓ) for the various models. For the dynamically consistent model with strain gradients as well as acceleration gradients we have taken $\ell_d^2/\ell_s^2 = 2$. It can be seen that the model with stable strain gradients leads to phase velocities that are larger than the elastic bar velocity c_e and they grow unbounded for the larger wave numbers, which is physically unrealistic. The model with unstable strain gradients exhibits a range of realistic phase velocities for wave numbers $k < 1/\ell$. However, for wave numbers $k > 1/\ell$ the phase velocity is imaginary. This implies that the response can grow unbounded without applying external work to the system, which is an indication of instability. The model with stress gradients and the model with acceleration gradients are denoted with a single curve in Fig. 2 (as explained above), and they show phase velocities that are bounded for all wave numbers, while they tend to zero for increasing wave numbers. The model that includes both strain gradients and acceleration gradients behaves qualitatively the same, except that a non-zero horizontal asymptote is approached for the larger wave numbers.

2.5.2. Two-dimensional case

The simplest format of the Mindlin model, given in Eq. (7), has three length scales, two of which are related to strain gradients whilst the third is related to acceleration gradients. In the dynam-

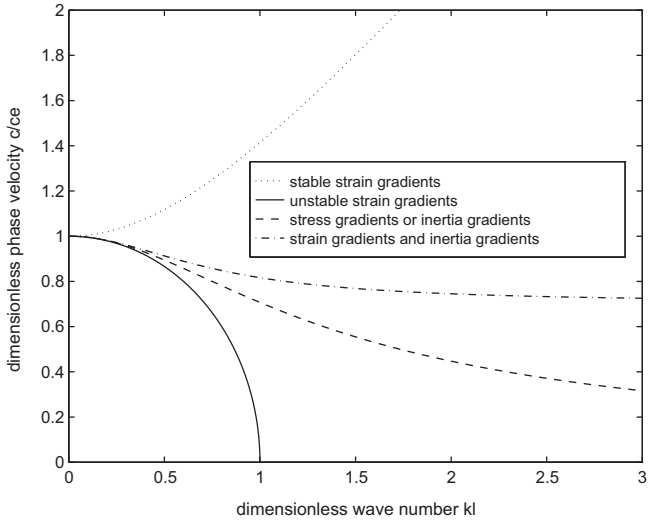

Fig. 2. Normalised phase velocity c/c_e versus normalised wave number ℓk for theories with stable strain gradients (dotted), unstable strain gradients (solid), stress gradients or inertia gradients (dashed) and strain gradients together with inertia gradients using $\alpha = 2$ (dash-dotted).

ically consistent model of Eq. (28) only two length scales are present: one related to strain gradients and one related to acceleration gradients. To assess the difference between Eqs. (7) and (28), two-dimensional wave propagation is studied. The two displacement components u_x and u_y are written in terms of a dilatational potential Φ and a distortional potential Ψ as

$$u_x = \Phi_{,x} + \Psi_{,y} \quad \text{and} \quad u_y = \Phi_{,y} - \Psi_{,x} \tag{37}$$

With these substitutions, Eq. (7) can be written as

$$\begin{bmatrix} \frac{\partial}{\partial x} \\ \frac{\partial}{\partial y} \end{bmatrix} \left\{ (\lambda+\mu)\left(\Phi_{,ii} - \ell_2^2 \Phi_{,iijj}\right) + \mu\left(\Phi_{,ii} - \ell_3^2 \Phi_{,iijj}\right) - \rho\left(\ddot{\Phi} - \ell_1^2 \ddot{\Phi}_{,ii}\right) \right\} + \begin{bmatrix} \frac{\partial}{\partial y} \\ -\frac{\partial}{\partial x} \end{bmatrix} \left\{ \mu\left(\Psi_{,ii} - \ell_3^2 \Psi_{,iijj}\right) - \rho\left(\ddot{\Psi} - \ell_1^2 \ddot{\Psi}_{,ii}\right) \right\} = \begin{bmatrix} 0 \\ 0 \end{bmatrix} \tag{38}$$

by which it follows that the two expressions in brackets must each be zero.

We substitute general harmonic waves via $\Phi = \widehat{\Phi} \exp(\mathrm{i}(k_x x + k_y y - \omega t))$ for the dilatational potential and $\Psi = \widehat{\Psi} \exp(\mathrm{i}(k_x x + k_y y - \omega t))$ for the distortional potential, whereby $\widehat{\Phi}$ and $\widehat{\Psi}$ are amplitudes whilst k_x and k_y are the wave numbers in the x and y direction. For compressive waves it is found that

$$\frac{c^2}{c_p^2} = \frac{1 + \frac{\lambda+\mu}{\lambda+2\mu}\ell_2^2 k^2 + \frac{\mu}{\lambda+2\mu}\ell_3^2 k^2}{1 + \ell_1^2 k^2} \tag{39}$$

and for shear waves we have

$$\frac{c^2}{c_s^2} = \frac{1 + \ell_3^2 k^2}{1 + \ell_1^2 k^2} \tag{40}$$

where $c_p = \sqrt{(\lambda+2\mu)/\rho}$ and $c_s = \sqrt{\mu/\rho}$ are the phase velocities of compressive waves and shear waves in classical elasticity; furthermore, $k = \sqrt{k_x^2 + k_y^2}$. Thus, for the general case that $\ell_2 \neq \ell_3$ the dispersion curve of compression waves differs from that of shear waves. However, if we take $\ell_2 = \ell_3$, it can be verified that the dispersion curves of compression waves and shear waves are the same.

3. Review of recent studies with unstable strain gradients

Gradient elasticity with unstable strain gradients is a popular tool for the description of dispersive waves, since many studies have related the unstable strain gradients to the underlying microstructure in an intuitively appealing and transparent manner as illustrated in Section 2.3.1. However, the use of unstable strain gradients may lead to anomalous conclusions. In this Section, we will discuss two recent studies that employ unstable strain gradients.

3.1. Discussion of the work of Maranganti and Sharma (2007)

Maranganti and Sharma (2007) have performed a comprehensive quantification of the constitutive parameters of gradient elasticity. They employed a molecular dynamics framework and fitted the gradient elasticity parameters from the numerical atomistic simulations for an impressive range of materials, including metals and polymers. As the starting point of their investigations, they postulated an energy density functional. The energy densities used for their version of gradient elasticity can be retrieved from Eq. (3) in Maranganti and Sharma (2007) as

$$\mathcal{T} = \frac{1}{2}\rho \dot{u}_i \dot{u}_i \tag{41}$$

for the kinetic energy density $\mathcal{T}$, and

$$\mathcal{U} = \frac{1}{2} C_{ijkl} u_{i,j} u_{k,l} + D_{ijklm} u_{i,j} u_{k,lm} + F^{(1)}_{ijklmn} u_{i,jk} u_{l,mn} + F^{(2)}_{ijklmn} u_{i,j} u_{k,lmn} \tag{42}$$

for the strain energy density $\mathcal{U}$, where the tensors D, $F^{(1)}$ and $F^{(2)}$ contain the higher-order contributions. Note that all higher-order terms appear in the strain energy – the kinetic energy retains its classical format, and consequently acceleration gradients are absent in this formulation.

Considering the "sign" paradox discussed in Section 2.3, Maranganti and Sharma (2007, p. 1840) attribute the dilemma partly to the "extreme simplicity of the strain-gradient models that are typically used", and they further suggest that the particular format of gradient elasticity they used avoids the stability constraints. The one-dimensional strain energy density following from Eq. (3) in Maranganti and Sharma (2007) reads

$$\mathcal{U} = \frac{1}{2} E u_{,x} u_{,x} + F^{(1)} u_{,xx} u_{,xx} + F^{(2)} u_{,x} u_{,xxx} \tag{43}$$

where we have left out contributions in terms of $u_{,x}u_{,xx}$. According to Maranganti and Sharma (2007, p. 1840), $F^{(1)}$ is required to be positive whereas "there is no such restriction on the tensor $F^{(2)}$". However, in our opinion it is necessary to constrain $F^{(2)}$ (taken as a scalar in the one-dimensional case), based on the following arguments.

3.1.1. Non-uniqueness of the higher-order contributions to the strain energy density

In contrast to the classical terms in the strain energy density, the higher-order contributions are non-unique. This has been noted by Maranganti and Sharma in the discussion of their Eq. (6c) and has also been addressed by Polizzotto (2003), Askes and Metrikine (2005) and Metrikine and Prokhorova (2010). In particular, contributions in terms of $F^{(1)}$ can be replaced by contributions in terms of $F^{(2)}$, and vice versa, which follows straightforwardly from integration by parts on a domain $0 \leqslant x \leqslant L$:

$$\int_0^L u_{,xx} u_{,xx} \mathrm{d}x = -\int_0^L u_{,x} u_{,xxx} \mathrm{d}x + [u_{,x} u_{,xx}]_0^L \tag{44}$$

Thus, the volumetric contributions of $F^{(1)}$ and $F^{(2)}$ to the strain energy can be exchanged, while the only difference concerns a contribution to the boundary conditions. In the light of this non-uniqueness of the strain energy density and to guarantee stability of the resulting model, it is necessary to require that $F^{(1)} - F^{(2)} > 0$.

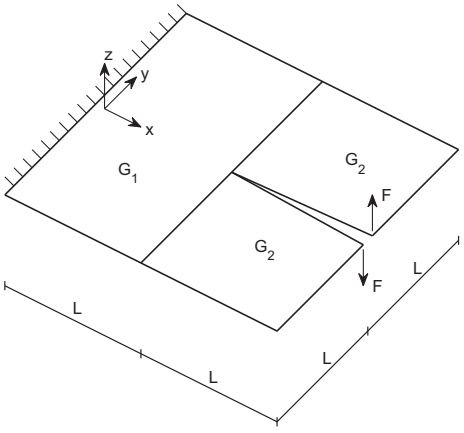

Fig. 3. Mode III fracture problem – geometry and boundary conditions for numerical simulations.

3.1.2. Instability of resulting governing equations

Using Eq. (43), the one-dimensional equation of motion is obtained as

$$\rho\ddot{u} = Eu_{,xx} - \frac{1}{2}\left(F^{(1)} - F^{(2)}\right)u_{,xxxx} \tag{45}$$

If no stability constraints are imposed on $F^{(2)}$, it would be possible that $F^{(2)} > F^{(1)}$. Defining an internal length scale ℓ via $\ell^2 = \frac{1}{2}\left(F^{(2)} - F^{(1)}\right)/E$, such a model would be unstable for wave numbers $k > 1/\ell$ in dynamics, as is shown in Section 2.5.1. Moreover, the response of a static boundary value problem would be non-unique for integer values of the ratio $L/2\pi\ell$, see for instance (Askes et al., 2002). In fact, Fig. 3 in Maranganti and Sharma (2007) exhibits the instability in dynamics: the dispersion curve (in terms of angular frequency rather than phase velocity) is first increasing, then decreasing and eventually crosses the horizontal axis. As mentioned in Section 2.5.1, for wave numbers $k > 1/\ell$ the angular frequency is imaginary, thus leading to an unbounded increase of the response in time.

Consequently, models according to Eq. (43) with $F^{(2)} > F^{(1)}$ are unstable. Furthermore, this cannot be mitigated by shifting contributions between $F^{(1)}$ and $F^{(2)}$ in Eq. (43). Maranganti and Sharma report their fitted constants of gradient elasticity in terms of a symmetrised tensor $f_{ijklmn} = F^{(2)}_{ijklmn} - F^{(1)}_{ijklmn}$. All tables in Maranganti and Sharma (2007) report positive values for f_{111111}, from which it follows that the gradient elasticity constants fitted by Maranganti and Sharma result in unstable models.

One could argue that these high wave numbers which would trigger instabilities are well beyond the first Brillouin zone and, thus, beyond the validity range of the model. Indeed, Maranganti and Sharma (2007, p. 1836) explicitly indicate that they fitted the constitutive constants of gradient elasticity for very small wave numbers only. However, in numerical simulations all wave numbers may be present in the signal, and a continuum model should in our opinion be stable for all wave numbers, be they inside or outside the Brillouin zone.

Remark 6. The non-uniqueness of the strain energy density of gradient elastic media has been discussed by Metrikine and Prokhorova (2010). Based on symmetry of stresses and relations between standard stresses and higher-order stresses, they conclude that the energy density of a gradient elastic material should not contain products of first-order and third-order displacement derivatives; instead, such contributions should be recast as products of second-order and second-order displacement derivatives. This would resolve the dilemma between $F^{(1)}$ and $F^{(2)}$, as all higher-order contributions should then appear in $F^{(1)}$, not $F^{(2)}$.

Remark 7. Despite the criticism expressed above, we do believe that the results of Maranganti and Sharma are extremely useful. One could simplistically say that they used dispersion to obtain length scales, instead of using length scales to obtain dispersion. Thus, the particular format of gradient elasticity is perhaps of lesser importance, and the calculated values of the internal length scales can be straightforwardly used in other formats of gradient elasticity. For instance, unstable strain gradients can be simply translated into stable inertia gradients with Eq. (27) or into stable stress gradients with Eq. (25).

Remark 8. In a more recent paper, Jakata and Every (2008) fit the constitutive parameters of gradient elasticity by means of experimental data. They use the same gradient elasticity formulation as Maranganti and Sharma, i.e. the one with unstable strain gradients, although they performed their fitting procedure over a larger range of wave numbers. Significantly, they report positive values for f_{111111} (which has the same meaning in their work as in the work of Maranganti and Sharma). Thus, our comments on the work of Maranganti and Sharma also apply to the work of Jakata and Every. However, we wish to express our appreciation of the formidable work carried out and, as above, suggest that the results be used in equivalent gradient elasticity theories with stable inertia gradients or stable stress gradients.

3.2. Discussion of the work of Wang, Guo and Hu (2008)

In order to describe wave dispersion in carbon nano-tubes (CNTs), Wang et al. (2008) formulated a gradient-enriched Timoshenko beam theory and a gradient-enriched shell theory. In both cases, gradient elasticity with unstable strain gradients was used, in particular Eq. (23). One of the main conclusions of Wang and coworkers is that a cut-off wave number exists beyond which the group velocity (that is, the propagation speed of the energy) is imaginary. Moreover, the cut-off frequency for the group velocity as reported by Wang and coworkers is different from the cut-off frequency for the angular frequency. This is an unusual observation, since the group velocity is the derivative of the angular frequency with respect to the wave number, and one would normally expect that the angular frequency and the group velocity are imaginary for the same range of wave numbers.

Below, we will show that the appearance of a cut-off frequency is due to the use of unstable strain gradients. This will be demonstrated for Euler–Bernoulli beam theory and illustrated for Timoshenko beam theory, both of which are enriched with combined strain/acceleration gradients. We will also show that for the case of unstable strain gradients the cut-off frequencies for angular frequency and group velocity coincide. Here, we will not carry out a detailed comparison between the two beam theories and the various gradient formulations – this has been done elsewhere (Askes and Aifantis, 2009). The main conclusions were, firstly, that the dynamically consistent model is the most suitable to describe flexural wave dispersion in CNTs; secondly, using dynamically consistent gradient elasticity allows for excellent fits with molecular dynamics simulations, irrespective of whether Euler–Bernoulli beam theory or Timoshenko beam theory is used.

3.2.1. Euler–Bernoulli beam theory

In Euler–Bernoulli beam theory, the transverse equation of motion without distributed forces is written as

$$\rho A\ddot{u}_y = M_{,xx} \tag{46}$$

where A is the cross-sectional area and M is the bending moment. The longitudinal direction of the beam is denoted with x whereas y denotes the transversal direction. Using combined strain/acceleration gradients, the longitudinal normal stress can be written as

$$\sigma = E\left(\varepsilon - \ell_s^2\varepsilon_{,xx}\right) + \rho\ell_d^2\ddot{\varepsilon} \tag{47}$$

The bending moment can then be expressed as

$$M = \int_A \sigma y \mathrm{d}A = EI\left(\kappa - \ell_s^2\kappa_{,xx}\right) + \rho I\ell_d^2\ddot{\kappa} \tag{48}$$

where $I = \int_A y^2 \mathrm{d}A$ is the second moment of area, $\kappa = -u_{y,xx}$ is the curvature, and $\varepsilon = \kappa y$. The transverse equation of motion is found as

$$\rho A\ddot{u}_y = -EI\left(u_{y,xxxx} - \ell_s^2 u_{y,xxxxxx}\right) - \rho I\ell_d^2\ddot{u}_{y,xxxx} \tag{49}$$

A general harmonic solution $u_y = \hat{u}_y \exp(\mathrm{i}(kx - \omega t))$ is substituted, so that Eq. (49) leads to

$$\omega = c_e R k^2 \sqrt{\frac{(1 + \ell_s^2 k^2)}{\left(1 + R^2\ell_d^2 k^4\right)}} \tag{50}$$

where again $c_e = \sqrt{E/\rho}$ and $R = \sqrt{I/A}$ is the gyration radius. The group velocity c_g is defined as $c_g = \partial\omega/\partial k$, which after some algebra can be written in normalised format as

$$\frac{c_g}{c_e} = Rk\,\frac{2+3\ell_s^2k^2+R^2\ell_s^2\ell_d^2k^6}{(1+\ell_s^2k^2)^{1/2}\left(1+R^2\ell_d^2k^4\right)^{3/2}} \tag{51}$$

The model with unstable strain gradients, as used by Wang and coworkers, is found by taking $\ell_d = 0$ and replacing ℓ_s^2 by $-\ell^2$. It can be seen from Eqs. (50) and (51) that both the angular frequency and the group velocity become imaginary (and, therefore, destabilising) for $k > 1/\ell$. Conversely, taking $\ell_s > 0$ and $\ell_d > 0$ prohibits imaginary values for ω and c_g.

3.2.2. Timoshenko beam theory

For the Timoshenko beam theory we use Eq. (47) and a similar expression for the shear stress τ, that is

$$\tau = G\left(\gamma - \ell_s^2\gamma_{,xx}\right) + \rho\ell_d^2\ddot{\gamma} \tag{52}$$

where G is the shear modulus and γ is the shear strain. The rotation of the cross section ϕ is given by $\phi = u_{y,x} - \gamma$. Using $\varepsilon = -\phi_{,x}y$, the bending moment is expressed in terms of ϕ as

$$M = -EI\left(\phi_{,x} - \ell_s^2\phi_{,xxx}\right) - \rho I\ell_d^2\ddot{\phi}_{,x} \tag{53}$$

For the shear force Q we have

$$Q = GA\beta\left(u_{y,x} - \phi - \ell_s^2u_{y,xxx} + \ell_s^2\phi_{,xx}\right) + \rho A\beta\ell_d^2\left(\ddot{u}_{y,x} - \ddot{\phi}\right) \tag{54}$$

where β is the Timoshenko shape factor of the cross section, which for thin-walled circular cross section equals $\beta = \frac{1}{2}$. The equation of transverse motion is thus written as

$$\rho A\ddot{u}_y = Q_{,x} = GA\beta\left(u_{y,xx} - \phi_{,x} - \ell_s^2u_{,yxxxx} + \ell_s^2\phi_{,xxx}\right) + \rho A\beta\ell_d^2\left(\ddot{u}_{y,xx} - \ddot{\phi}_{,x}\right) \tag{55}$$

and the equation of rotational motion reads

$$\begin{aligned}\rho I\ddot{\phi} = Q - M_{,x} &= GA\beta\left(u_{y,x} - \phi - \ell_s^2u_{y,xxx} + \ell_s^2\phi_{,xx}\right) + \rho A\beta\ell_d^2\left(\ddot{u}_{y,x} - \ddot{\phi}\right)\\ &\quad + EI\left(\phi_{,xx} - \ell_s^2\phi_{,xxxx}\right) + \rho I\ell_d^2\ddot{\phi}_{,xx}\end{aligned} \tag{56}$$

We substitute $u_y = \hat{u}_y\exp(\mathrm{i}(kx-\omega t))$ as well as $\phi = \hat{\phi}\exp(\mathrm{i}(kx-\omega t))$. The two equations of motion (55) and (56) accordingly lead to

$$\begin{aligned}&\left[\omega^2\rho A(1+\beta\ell_d^2k^2) - GA\beta k^2(1+\ell_s^2k^2)\right]\hat{u}_y\\ &\quad = \left[GA\beta(1+\ell_s^2k^2) - \omega^2\rho A\beta\ell_d^2\right]\mathrm{i}k\hat{\phi}\end{aligned} \tag{57}$$

and

$$\begin{aligned}&\left[\omega^2\left(\rho I + \rho A\beta\ell_d^2 + \rho I\ell_d^2k^2\right) - GA\beta(1+\ell_s^2k^2) - k^2EI(1+\ell_s^2k^2)\right]\mathrm{i}k\hat{\phi}\\ &\quad = \left[GAk^2\beta(1+\ell_s^2) - \omega^2\rho A\beta\ell_d^2k^2\right]\hat{u}_y\end{aligned} \tag{58}$$

For non-zero amplitudes $\hat{u}_y$ and $\hat{\phi}$ it is then found that

$$\begin{aligned}&\frac{\omega^4}{k^4c_e^4}\left[(1+\ell_d^2k^2)(1+\beta\ell_d^2k^2) + \frac{A}{Ik^2}\beta\ell_d^2k^2\right]\\ &\quad - \frac{\omega^2}{k^2c_e^2}\left[\frac{GA\beta}{EIk^2} + 1 + \beta\ell_d^2k^2 + \frac{G\beta}{E}(1+\ell_d^2k^2)\right]\cdot(1+\ell_s^2k^2)\\ &\quad + \frac{G\beta}{E}(1+\ell_s^2k^2)^2 = 0\end{aligned} \tag{59}$$

Resolving Eq. (59) for the angular frequency ω leads to lengthy closed-form expressions which hardly offer any insight; this holds even more for the group velocity c_g which is the derivative of ω. For this reason, they are not reproduced here. However, the special case of unstable strain gradients ($\ell_d = 0, \ell_s^2 = -\ell^2$) and thin-walled cross section ($\beta = \frac{1}{2}$) is elaborated further, and we will also assume that Poisson's ratio $\nu = \frac{1}{5}$ as suggested by Wang et al. (2008). With these specifications an expression for the angular frequency is found as

$$\omega = c_ek\sqrt{1-\ell^2k^2}\cdot\sqrt{\frac{5+29R^2k^2 \pm \sqrt{25+290R^2k^2+361R^4k^4}}{42R^2k^2}} \tag{60}$$

where again the radius of gyration $R = \sqrt{I/A}$. The group velocity associated with the lower angular frequency branch (and normalised with c_e) is given by

$$\begin{aligned}\frac{c_g}{c_e} = &\frac{(1-\ell^2k^2)\left(58R^2k - \frac{290R^2k+722R^4k^3}{\sqrt{25+290R^2k^2+361R^4k^4}}\right)}{\sqrt{192R^2(1-\ell^2k^2)\left(5+29R^2k^2-\sqrt{25+290R^2k^2+361R^4k^4}\right)}}\\ &- \frac{2\ell^2k\left(5+29R^2k^2-\sqrt{25+290R^2k^2+361R^4k^4}\right)}{\sqrt{192R^2(1-\ell^2k^2)\left(5+29R^2k^2-\sqrt{25+290R^2k^2+361R^4k^4}\right)}}\end{aligned} \tag{61}$$

Although Eq. (60) and, in particular, Eq. (61) are lacking in transparency, an important observation is that the only parameter set that leads to imaginary solutions is $k > 1/\ell$; this holds for the angular frequency as well as for the group velocity.

3.2.3. Critique

The observation of Wang and coworkers that is most relevant to the context of this paper is the *appearance* of cut-off wave numbers as such, which is undesirable as they are an indication of instability. Although we argue that cut-off wave numbers can be avoided by an appropriate choice of gradient enrichment, we also comment on the *coincidence* (or otherwise) of the cut-off wave numbers for the angular frequency and the group velocity.

The appearance of cut-off wave numbers is a central theme in the study of Wang and coworkers, but it must be realised that this is not an intrinsic property of all formats of gradient elasticity. Instead, cut-off wave numbers are the consequence of one particular type of gradient enrichment, namely unstable strain gradients. The use of stable strain gradients combined with acceleration gradients avoids all cut-off wave numbers, which is clearly demonstrated for the Euler–Bernoulli beam theory in Eqs. (50) and (51). For the Timoshenko beam theory, we have provided solutions for the angular frequency in (Askes and Aifantis, 2009) which demonstrate that cut-off frequencies do not occur if combined strain/inertia gradients are used.

The results presented by Wang and coworkers indicate that the cut-off wave number of the angular frequency is significantly different from the cut-off wave number of the group velocity. This is reported for unstable strain gradients used in shell theory and in Timoshenko beam theory (Wang et al., 2008). However, this difference does not appear in our derivations; rather, the cut-off wave number (beyond which instabilities are triggered) is the same for the angular frequency and the group velocity. Given that the group velocity is the derivative of the angular frequency, one would expect that they are imaginary for the same range of wave numbers.

Wang et al. (2008, p. 1437) suggest that the appearance of a cut-off frequency in the group velocity offers an explanation why molecular dynamics results are unavailable for wave numbers larger than this cut-off wave number. As we have mentioned above, the appearance of a cut-off wave number is an artefact of the particular format of gradient elasticity equipped with unstable strain

gradients. Since cut-off wave numbers are absent in most formats of gradient elasticity, their association with inavailability of molecular dynamics results should, in our opinion, be treated with reservation.

4. Identification and quantification of length scale parameters

One of the main issues of gradient theories in general, and gradient elasticity theories in particular, is the identification of the length scale parameters. It is normally assumed that these length scale parameters are some representation of the material's microstructure, but a more quantitative approach is desired for the application of gradient elasticity to practical problems. In this Section, we will summarise various strands of research efforts aimed at the identification and quantification of the gradient elasticity constants. As it turns out, a recurrent trend is that the length scale parameters are related to the heterogeneity of the material.

4.1. Relation with size of representative volume elements

An alternative approach to describe the response of heterogeneous materials is homogenising the response of a Representative Volume Element (RVE). An RVE is usually defined at the microlevel of observation as a cell large enough for the response to be statistically homogeneous. For periodic microstructures the RVE is the unit cell, whilst for randomly heterogeneous materials the RVE is theoretically infinitely large but in practice taken as the smallest size for which the response is statistically homogeneous *within user-defined error thresholds* (Ostoja-Starzewski, 2002).

The size of the RVE, denoted as L_{RVE}, is obviously a parameter with the unit of length, and a pertinent question is whether the RVE size can be related to the length scale parameters of gradient theories. Nested finite element solution procedures have been formulated in which the constitutive response at the macroscopic level is determined by solving a boundary volume problem on an RVE at the microscopic level. A recent addition has been to include higher order gradients in this scale transition, resulting in so-called *second-order homogenisation schemes* (Kouznetsova et al., 2002, 2004a). It has been demonstrated that such a scheme automatically leads to a gradient theory in the spirit of Eq. (12) on the macroscopic level in which the length scale parameter ℓ is found in terms of the RVE size (Kouznetsova et al., 2004b; Gitman et al., 2004). Both Gitman et al. (2004) and Kouznetsova et al. (2004b) found that $\ell^2 = \frac{1}{12} L_{\mathrm{RVE}}^2$, although the latter study assumes a homogeneous material for which the RVE size is theoretically zero. If such an approach is extended to dynamics, the dynamically consistent gradient elasticity theory of Eq. (28) is obtained whereby the coefficients of strain gradients and acceleration gradients are related to the static RVE size and the dynamic RVE size, respectively (Gitman et al., 2005, 2007a).

In this approach, the question "how large is the length scale?" is in fact rephrased as "how large is the RVE size?" Many studies have been devoted to the quantification of RVE sizes for randomly heterogeneous materials, and the general trends are that the RVE size increases with increased contrast in material properties, see for instance (Kanit et al., 2003; Gitman et al., 2006). In a related fashion, statistically inhomogeneous elastic media have been considered where Taylor series expansions for random fields result in gradient elasticity models as given in Eq. (12) with the internal length scale ℓ depending on the correlation properties of the medium (Frantziskonis and Aifantis, 2002; Aifantis, 2003).

Remark 9. An unresolved issue in this line of thinking is the treatment of materials that exhibit *strain-softening*. On the one hand, it has been shown on many occasions that the inclusion of length scale parameters is essential to capture the physics of the problem and to maintain well-posedness of its mathematical description, see for instance (de Borst et al., 1995) and references cited therein. On the other hand, it has also been demonstrated that RVEs do not exist for softening materials, by which the concept of RVE size (and its relation to the length scales of gradient theories) becomes meaningless (Gitman et al., 2007b) and other micro–macro relations must be explored (Gitman et al., 2008).

4.2. Closed-form solutions

Over the years, several procedures have been suggested to derive the gradient elasticity constants from the constitutive properties of a composite material or an equivalent discrete model of masses and springs. For composite materials, the gradient elasticity length scale parameters are normally found to be increasing with increasing contrast in material properties between the constituents. In case the response of a discrete model is continualised, the length scales of gradient elasticity are usually related to the particle spacing of the discrete model (see also Section 2.3.1).

4.2.1. Strain gradients obtained through mixture theory

On a nanoscopic scale one may distinguish between atoms that are placed in the interior of a grain and atoms that are located on the grain boundary. Under certain kinematic and dynamic constraints, the elastic governing equations turn out to be of the gradient type, and the material parameters can be related to the parameters of the two phases (interior and boundary) as well as their interaction forces (Altan and Aifantis, 1997; Aifantis, 2000). The two phases are indicated with superscripts a and b and assumed to behave elastically. The divergence of stress in each phase is thus written as

$$\sigma_{ij,j}^a = (\lambda^a + \mu^a) u_{j,ij}^a + \mu^a u_{i,jj}^a \tag{62}$$

$$\sigma_{ij,j}^b = (\lambda^b + \mu^b) u_{j,ij}^b + \mu^b u_{i,jj}^b \tag{63}$$

where λ and μ indicate the Lamé constants for each phase. The interaction between the two phases is assumed to be governed by an internal body force proportional to an interaction stiffness K, that is

$$\sigma_{ij,j}^a = K(u_i^a - u_i^b) \tag{64}$$

$$\sigma_{ij,j}^b = K(u_i^b - u_i^a) \tag{65}$$

From Eqs. (62) and (64) an expression for u^b can be found; similarly, u^a can be obtained by combining Eqs. (63) and (65). Hence,

$$u_i^a = u_i^b - \frac{\lambda^b + \mu^b}{K} u_{j,ij}^b - \frac{\mu^b}{K} u_{i,jj}^b \tag{66}$$

$$u_i^b = u_i^a - \frac{\lambda^a + \mu^a}{K} u_{j,ij}^a - \frac{\mu^a}{K} u_{i,jj}^a \tag{67}$$

Next, the expression for u^a is substituted back into Eqs. (62) and (64); likewise, the expression for u^b is substituted into Eqs. (63) and (65). These two results are added up, which yields

$$(\lambda^a + \mu^a + \lambda^b + \mu^b) u_{j,ij} + (\mu^a + \mu^b) u_{i,jj} - \frac{\lambda^a \lambda^b + 2\lambda^a \mu^b + 2\lambda^b \mu^a + 3\mu^a \mu^b}{K} u_{j,ijkk} - \frac{\mu^a \mu^b}{K} u_{i,jjkk} = 0 \tag{68}$$

where the average displacements $u_i \equiv \frac{1}{2}(u_i^a + u_i^b)$. Yet again, the higher-order terms are found to be the Laplacian of the lower-order terms. In fact, it can be verified that Eq. (68) is the static version of the Mindlin model given in Eq. (7), whereby the two length scales ℓ_2 and ℓ_3 are given by

$$\ell_2 = \sqrt{\frac{\lambda^a\lambda^b + 2\lambda^a\mu^b + 2\lambda^b\mu^a + 3\mu^a\mu^b}{K\left(\lambda^a + \mu^a + \lambda^b + \mu^b\right)}} \quad \text{and} \quad \ell_3 = \sqrt{\frac{\mu^a\mu^b}{K(\mu^a + \mu^b)}} \tag{69}$$

For general constitutive parameters of the two phases it will hold that $\ell_2 \neq \ell_3$. Aifantis' theory with $\ell_2 = \ell_3$ is retrieved for the special case that

$$\lambda^i = -\frac{\mu^i(2\mu^i\mu^j + 2\mu^j\mu^j + \lambda^j\mu^i)}{\mu^i\mu^j + \lambda^j\mu^i + \lambda^j\mu^j + 2\mu^j\mu^j} \tag{70}$$

where $i = a$ and $j = b$ or vice versa.

4.2.2. Continualisation of a periodic discrete lattice

In Section 2.3.1 the most straightforward continualisation method has been discussed and it was shown that the resulting higher-order strain gradients are destabilising. In recent years, more sophisticated continualisation procedures have been suggested that avoid the instabilities discussed in Section 2.3.1.

Ioannidou et al. (2001) suggested to continualise a discrete medium where nearest neighbour interaction takes place with positive elastic spring stiffness and next-nearest neighbour interaction is governed by negative elastic spring stiffnesses. With an appropriate selection of parameters this results in a gradient elasticity formulation with stable strain gradients. However, for completeness it must be mentioned that this concerns a model with unstable strain gradients (related to positive spring stiffnesses) as well as stable strain gradients (related to negative spring stiffnesses) with the latter outweighting the former. This seems quite a restrictive assumption and may not be generally representative for many materials. It is also mentioned that with the dominance of stable strain gradients over unstable strain gradients unbounded phase velocities are found for the higher wave numbers, see Section 2.5.1.

Vasiliev et al. (2010) distinguish multiple displacement fields which are related hierarchically. In their continualisation approach, each displacement field is associated with a distinct range of wave numbers, by which an improved correspondence with discrete lattice models can be obtained.

Metrikine and Askes (2002, 2006) suggested an alternative continualisation method that relaxes the kinematic link between discrete model and continuum model as described in Section 2.3.1. In their approach, the continuum displacement is not linked one-to-one with the discrete particle displacement at the same location, but instead as the weighted average of the displacements of multiple particles in a (limited) neighbourhood around the same location. With the notation of Section 2.3.1 (and thus assuming one spatial dimension – see (Metrikine and Askes, 2006) for the two-dimensional version), this approach can be described by

$$u(x,t) = \frac{au_{n+1}(t) + u_n(t) + au_{n-1}(t)}{1 + 2a} \tag{71}$$

which defines the continuum displacement $u(x,t)$ as the weighted average of the three discrete particle displacements u_{n+1}, u_n and u_{n-1}, where a is a dimensionless weighting constant. After some lengthy but straightforward derivations, a dynamically consistent gradient elasticity model with strain gradients and acceleration gradients is obtained (Metrikine and Askes, 2002), that is

$$E\left(u_{,xx} - \frac{10a - 1}{12(1 + 2a)}d^2u_{,xxxx}\right) = \rho\left(\ddot{u} - \frac{1}{1 + 2a}d^2\ddot{u}_{,xx}\right) \tag{72}$$

The coefficients accompanying the higher-order gradients are thus found in closed form in terms of the particle spacing d and the weighting constant a. Nevertheless, the meaning of the weighting constant is less clear than that of the particle spacing.

Remark 10. Eq. (72) can be seen as a unification of the theory with unstable strain gradients and the theory with inertia gradients. For $a = 0$ Eq. (71) reduces to the standard continualisation assumption of Section 2.3.1 and, consequently, Eq. (72) becomes identical to Eq. (22). Conversely, taking $a = \frac{1}{10}$ means that the strain gradients disappear from Eq. (72) and the format of Eq. (27) is retrieved. The method of alternative continualisation is related to asymptotic equivalence of gradient series as explored by Pichugin et al. (2008).

4.2.3. Homogenisation of a laminate

Fish and co-workers studied dispersive wave propagation through laminated composites and they applied homogenisation with multiple length scales and time scales to arrive at a gradient elasticity theory with unstable strain gradients, which were afterwards rewritten as stable inertia gradients (Chen and Fish, 2001; Fish et al., 2002b,a). Interestingly, the obtained internal length scale ℓ was expressed in terms the constituents' volume fractions and material properties (and in particular the *contrast* in material properties). This problem was also studied more recently by Andrianov et al. (2008, 2010a), who obtained similar results.

Denoting the two constituents with superscripts a and b, a periodic laminate with unit cell size d is taken. The volume fractions are α and $(1 - \alpha)$ for phases a and b, respectively. The effective mass density ρ and effective Young's modulus E were found as Chen and Fish (2001)

$$\rho = \alpha\rho^a + (1 - \alpha)\rho^b \quad \text{and} \quad E = \frac{E^aE^b}{(1 - \alpha)E^a + \alpha E^b} \tag{73}$$

The obtained gradient-enriched equation of motion reads

$$E\left(u_{,xx} + \frac{1}{12}\gamma d^2u_{,xxxx}\right) = \rho\ddot{u} \tag{74}$$

where the dimensionless coefficient γ captures the contrast in acoustic impedance and is given by Chen and Fish (2001)

$$\gamma = \left(\frac{\alpha(1 - \alpha)\left(E^a\rho^a - E^b\rho^b\right)}{\rho\left((1 - \alpha)E^a + \alpha E^b\right)}\right)^2 \tag{75}$$

The instability of Eq. (74) was acknowledged and it was suggested to translate the unstable strain gradients into stable inertia gradients (Chen and Fish, 2001), similar to the technique discussed in Section 2.3.2.

The results of Fish and coworkers were used more recently to quantify the higher-order coefficients of a one-dimensional version of Eq. (28) (Bennett et al., 2007). A key assumption in this study was to use the link between the static length scale ℓ_s and the static RVE size as explained in Section 4.1 – for a periodic laminate the static RVE size $L_{\text{stat}} \equiv d$. After a bit of straightforward algebra, the two length scale parameters ℓ_s and ℓ_d were obtained as Bennett et al. (2007)

$$\ell_s = \frac{1}{\sqrt{12}}d \quad \text{and} \quad \ell_d = \sqrt{\frac{\gamma + 1}{12}}d \tag{76}$$

that is, both length scales are expressed in terms of the microstructural constituents and geometry, without any free parameter. Fish et al. (2002a) have also suggested multi-dimensional extensions of Eq. (74) and its counterpart with stable inertia gradients.

4.3. Quantification of length scales

So far, we have discussed how to relate the length scales of gradient elasticity to other constitutive or geometrical properties of the material, which could be termed "identification of length scales". However, there are also a number of studies devoted to obtaining numerical values for the length scales, or in other words

the "quantification of length scales." The methods used in these studies are either experimental validation or validation through nanoscale simulation techniques such as lattice dynamics or molecular dynamics (MD).

4.3.1. Experimental validation

As mentioned in the Introduction, the robust and simple gradient elasticity models with one additional parameter were proposed to interpret deformation phenomena that could not be captured by classical theory, such as necking and the formation of shear bands, as well as the occurrence of size effects. Similarly, in dynamics such simple theories were used to capture the effects of dispersive waves. It was thus necessary to check the validity of the models against the corresponding experimental data and also in relation to the reasonableness of the values obtained for the coefficients of the newly introduced higher-order terms, that is the length scale parameters. In gradient plasticity the shear band widths and spacings were determined in relation to a value of the internal length that was directly related to the grain size for polycrystalline specimens or the dislocation spacing/source distance of single crystals. The same was true for size effect interpretations of plastically twisted microwires of varying diameter or plastically bent microbeams of varying thickness, as well as for micro/nano indentations where the hardness varied as a function of indentation depth.

In gradient elasticity, various estimates were obtained from dispersive wave characteristics. Dispersion of various types of waves has been established for many microstructured materials, see for instance the studies of the 1960s and early 1970s (Yarnell et al., 1964b,a; Warren et al., 1967; Verble et al., 1968; Price et al., 1971). A rudimentary gradient elasticity interpretation of experimentally obtained ultrasonic wave dispersion results in metals was given by Savin et al. (1970). More recent efforts cover a vast range of scales, including those of Stavropoulou et al. (2003) for marble, Jakata and Every (2008) for a number of cubic crystals, and Erofeyev (2003) for a range of metals – see also the references cited therein. Furthermore, size effect measurements of torsion and bending were performed of specimens made from materials with a dominant microstructure, such as bones and foams where the length scale parameter was related to the average cell size. Details on these can be found in Aifantis (1999, 2003), where also some comments on the physical background of the length scale parameters are provided.

More recently, the robust and simple gradient elasticity model of Aifantis was used to describe characteristics at the atomic scale, such as dislocation core sizes, as well as to interpret measurements pertaining to the dislocation density tensor and internal strain states through X-ray profile analysis (Kioseoglou et al., 2006, 2008, 2009; Aifantis, 2009a). The length scale parameter values estimated from these measurements are directly related to the lattice spacing, as expected. In these papers, atomistic computer simulations are also presented based on MD potentials and it shown that the simple gradient elasticity model is indeed superior to such simulations which become very difficult to carry out in the proximity of the dislocation line.

Further results have been obtained by Lam et al. (2003), who used a re-formulation of the Mindlin theory that, when applied to beam theory, is governed by a single independent length scale parameter. The experimentally obtained value for this length scale is in the order of microns for an epoxy beam and may be considered to be somewhat high, but this could potentially be related to the particular boundary value problem that is considered and how gradient effects are activated under these boundary conditions.

4.3.2. Nanoscale numerical simulations

Opie and Grindlay (1972) postulated a Lennard–Jones potential for lattices consisting of noble gas solids argon, krypton and xenon close to a temperature of 0 K. They also assumed linear elastic equations of motion with strain gradients but without inertia gradients. The Lennard–Jones potential has two free parameters, and by comparing the dynamic response of the lattice with that of the gradient elastic continuum all constitutive coefficients (classical as well as higher-order) were found in terms of these two parameters. Thus, assuming that the classical constitutive elastic constants can be fitted from experiments, the higher-order constitutive constants are found as well. DiVicenzo (1986) followed a similar procedure but focussed on gallium-arsenic, which is anisotropic. Similar to the study by Opie and Grindlay, strain gradients were included but inertia gradients were ignored. One of the manifestations of anisotropy was the appearance of spatial displacement derivatives of odd order. The various higher-order stiffness tensors of the gradient-enriched continuum were again found by comparison with the response of the lattice model.

Wang and Hu (2005) simulated the propagation of flexural waves in carbon nanotubes (CNTs) by means of MD and with beam theories. They used Euler–Bernoulli and Timoshenko beam theories extended with unstable strain gradients. The length scale was related directly to the interatomic spacing via the procedure described in Section 2.3.1, and as such no fitting procedure was used to quantify the length scale from the MD results. Nevertheless, the results of gradient elastic Timoshenko beam theory were in good agreement with the MD results, although the use of unstable strain gradients implies that the model should not be used beyond a certain cut-off wave number. Moreover, the results obtained with Euler beam theory are much further removed from the MD results (Wang and Hu, 2005). Duan et al. (2007) used MD simulations to fit the length scale parameter of the Eringen model in Timoshenko beam theory. The fits were carried out for the first four eigenfrequencies of beams with either clamped–clamped or clamped-free boundary conditions. The best fit of the length scale parameter was usually found (i) to decrease somewhat with increasing mode number (with one exception), and (ii) to decrease importantly with increasing slenderness, i.e. the ratio of CNT length over CNT radius.

The findings of Wang and Hu (2005) were revisited more recently by the authors of the present article (Askes and Aifantis, 2009), whereby the two beam theories were enriched with unstable strain gradients, stress gradients, inertia gradients and the dynamically consistent combination of stable strain gradients with inertia gradients. In particular the dynamically consistent gradient elasticity model leads to results that show an excellent fit with the MD results of Wang and Hu; interestingly, this holds not only for the Timoshenko beam theory but also for the Euler–Bernoulli beam theory (Askes and Aifantis, 2009). A rudimentary fit of the dynamic length scale ℓ_d of dynamically consistent gradient elasticity was carried out to match the results of beam theories with those of MD. It was found that the dynamic length scale ℓ_d scales more or less with the radius of the CNT, and it is significantly larger in Euler–Bernoulli beam theory than in Timoshenko beam theory (Askes and Aifantis, 2009).

Maranganti and Sharma (2007) used three methods to simulate the material behaviour at the nanoscale, namely empirical lattice dynamics (similar to the work of DiVicenzo mentioned above), ab initio lattice dynamics and empirical MD. Obtained values for the length scales are typically in the order of magnitude of $10^{-10} - 10^{-9}$ m for a variety of materials, ranging from metals to polymers.

5. Numerical implementations

Gradient elasticity has not yet found the widespread dissemination in practical applications that would be warranted by its theoretical foundations. One of the main reasons is that

straightforward, robust numerical implementations of gradient elasticity were lacking until recently. In particular *finite element* implementations must be provided for a material model to be used widely. Most finite element formulations are based on the assumption that the partial differential equations (p.d.e.) to be discretised have at most second-order derivatives with respect to the spatial coordinates. Discretisation of such second-order p.d.e. requires continuity of the primary unknowns (here: displacements) but not of their spatial derivatives – this is denoted as $\mathcal{C}^0$-continuity. In contrast, the fourth-order spatial derivatives such as those given in Eq. (7) require $\mathcal{C}^1$-continuity whereby both the primary unknowns and their spatial derivatives are continuous.

Certain authors have used meshless methods for the implementation of gradient elasticity, by which $\mathcal{C}^1$-continuity is easily accomodated (Askes and Aifantis, 2002; Tang et al., 2003; Sansour and Skatulla, 2009). Boundary element implementations for gradient elasticity have also been developed, in particular by Tsepoura et al. (2002), Polyzos et al. (2003), Tsepoura et al. (2003), Polyzos et al. (2005), Karlis et al. (2007). However, in this Section we will focus on finite element implementations. After a brief overview of finite element strategies, we will discuss the simplest implementations for most of the main formats of gradient elasticity treated in Section 2. Another obstacle to a wider dissemination of gradient theories has been a lack of agreement on which boundary conditions should be used. Since this is closely related to finite element implementations, in that variationally consistent formats of boundary conditions must be taken, this issue is addressed here as well.

5.1. Overview of finite element implementations

Roughly, two classes of finite element implementation strategies for gradient elasticity can be distinguished, which are based on *next nearest neighbour interaction* or on the *discretisation of multiple fields*. Higher-order continuity can be attained by dropping the usual finite element property that nodes only interact with each other if they are attached to the same element. Thus, "nearest neighbour interaction" is given up for "next nearest neighbour interaction" to attain $\mathcal{C}^1$-continuity. This is the case, for instance, with novel discretisation techniques such as discontinuous Galerkin methods (Engel et al., 2002) and the subdivision surfaces paradigm (Cirak et al., 2000) – in fact, also the meshless methods mentioned above fall in this category. Although only the displacement field needs to be discretised, these approaches do not fit easily in standard finite element packages, that normally rely on nearest-neighbour interaction to enable an element-by-element assembly.

Alternatively, multiple fields (rather than the displacement field only) can be discretised. In this case, one should distinguish between (i) formats of gradient elasticity that lead to fourth-order p.d.e. in terms of displacements only, and (ii) formats of gradient elasticity that consist of second-order p.d.e. in terms of displacements and additional variables. Finite element strategies for gradient elasticity with fourth-order p.d.e. include the following.

- Hermitian finite elements are truly $\mathcal{C}^1$-continuous. The displacements as well as all first derivatives and some second derivatives are interpolated; the number of degrees of freedom per element normally increases by a factor four (Petera and Pittman, 1994) to six (Zervos et al., 2001). This approach has recently been extended to 3D (Papanicolopulos et al., 2009). It was also noted that although the number of degrees of freedom per element increases, the number of elements needed for a certain accuracy decreases due to the additional resolution provided by the interpolation of the displacement derivatives (Papanicolopulos et al., 2009).
- Mixed finite elements fulfill the continuity requirements only in a weak sense. Displacements and the first derivatives are interpolated; the number of degrees of freedom per element typically increases by a factor two (Shu et al., 1999; Matsushima et al., 2002; Kouznetsova et al., 2004a), three (Soh and Wanji, 2004) or four (Amanatidou and Aravas, 2002). Care may be required to ensure that the finite element passes several patch tests: a specific element might pass one patch test but fail another, compare for instance element QU54L16 from Shu et al. (1999) with element I-13-70 from Amanatidou and Aravas (2002).

Other formats of gradient elasticity consist of second-order p.d.e. in terms of the displacements and one or more other variables; these p.d.e. may be coupled or uncoupled.

- Zervos (2008) provided an implementation of Mindlin's theory of elasticity with microstructure, i.e. based on Eq. (3), whereby the primary unknowns are the displacements and the microdeformations. Interestingly, he also demonstrated that the response of gradient elasticity can be emulated with the same implementation by a specific choice of higher-order constitutive coefficients. Namely, the coefficients accompanying the *relative deformation* γ_{ij} as defined in Section 2.1 must be set very large so as to penalise the difference between micro-deformation and macro-deformation, by which the response of elasticity with microstructure reduces to the response of gradient elasticity (Zervos, 2008). The performance of this approach has been compared to that of Hermitian finite elements by Zervos et al. (2009).
- Askes and Gutiérrez (2006) developed an implementation of a variant of the Eringen theory discussed in Section 2.2.1. The interpolated unknowns are the displacements together with the nonlocal strains (rather than the nonlocal stresses), and it was shown that the interpolation polynomials of the displacements should be taken of lower degree than that of the nonlocal strains in order to avoid oscillations.
  Nevertheless, for optimal convergence rates (in the sense of error reduction for a uniform increase in number of elements) it is not sufficient to take the interpolations simply as, say, linear for the displacements and quadratic for the nonlocal strains. Although this topic has not been studied intensively in gradient elasticity, many attempts have been made in classical elasticity to implement finite elements with separate interpolations for stresses and displacements, see for instance (Arnold et al., 1984; Arnold and Winther, 2002) The resulting implementations tend to be complicated and involve, for instance, a mixture of nodal degrees of freedom, edge degrees of freedom and element degrees of freedom (Carstensen et al., 2008). This holds for classical elasticity, and it appears that the additional complication of gradient-enrichment will not result in less cumbersome implementations. Thus, a simple and straightforward implementation of the Eringen theory that provides optimal convergence has not been accomplished as yet, and may not be feasible.
- Some specific formats of gradient elasticity such as Eq. (12) allow for an operator-split as has been explored by Ru and Aifantis (1993). Instead of one set of fourth-order p.d.e., two sets of second-order p.d.e. are solved sequentially as outlined in Section 2.2.2. The number of degrees of freedom per element thus increases, but the two systems are formally decoupled and can be solved separately, which limits the computational costs involved (Tenek and Aifantis, 2002; Askes et al., 2008b). This approach for statics has inspired a similar solution strategy for dynamically consistent gradient elasticity given in Eq. (28), although the resulting equations are coupled rather than

uncoupled (Askes and Aifantis, 2006; Askes et al., 2007; Bennett and Askes, 2009).

In the next Section, we will discuss simple and effective C^0 finite element implementations of gradient elasticity with strain gradients, acceleration gradients, and the dynamically consistent combination of strain gradients with acceleration gradients.

5.2. Finite element equations

In this Section, we will depart from the index tensor notation used in the remainder of this paper and switch to matrix–vector notation. Furthermore, we will give the finite element equations for the 2D case, but extension to 3D is straightforward. Discretisation of the displacements is performed with shape functions N_i which are collected in a matrix $\mathbf{N}_u$, i.e. in 2D:

$$\mathbf{N}_u = \begin{bmatrix} N_1 & 0 & N_2 & 0 & \cdots \\ 0 & N_1 & 0 & N_2 & \cdots \end{bmatrix} \tag{77}$$

The continuum displacements $\mathbf{u} = [u_x, u_y]^T$ are related to the nodal displacements $\mathbf{d} = [d_{1x}, d_{1y}, d_{2x}, d_{2y}, \ldots]^T$ via $\mathbf{u} = \mathbf{N}_u\mathbf{d}$. Similar discretisations can be performed for other fields, such as the nonlocal strains or the nonlocal stresses. Furthermore, we define the usual derivative operators ∇ and $\mathbf{L}$ as

$$\nabla = \begin{bmatrix} \frac{\partial}{\partial x} \\ \frac{\partial}{\partial y} \end{bmatrix} \quad \text{and} \quad \mathbf{L} = \begin{bmatrix} \frac{\partial}{\partial x} & 0 \\ 0 & \frac{\partial}{\partial y} \\ \frac{\partial}{\partial y} & \frac{\partial}{\partial x} \end{bmatrix} \tag{78}$$

while also $\nabla^2 \equiv \nabla^T\cdot\nabla$.

5.2.1. Strain gradients

The Ru-Aifantis theorem discussed in Section 2.2.2 splits the original fourth-order p.d.e. of gradient elasticity into two sets of second-order p.d.e., the first of which are the p.d.e. of classical elasticity:

$$\mathbf{L}^T\mathbf{C}\mathbf{L}\mathbf{u}^c + \mathbf{b} = \mathbf{0} \tag{79}$$

where the body forces $\mathbf{b} = [b_x, b_y]^T$ and $\mathbf{C}$ is the matrix equivalent of the constitutive tensor C_{ijkl}. Taking the weak form of Eq. (79) with domain Ω and boundary Γ, followed by integration by parts, gives

$$\int_\Omega (\mathbf{L}\mathbf{w})^T\mathbf{C}\mathbf{L}\mathbf{u}^c \mathrm{d}\Omega = \int_\Omega \mathbf{w}^T\mathbf{b}\mathrm{d}\Omega + \int_{\Gamma_n} \mathbf{w}^T\mathbf{t}\mathrm{d}\Gamma \tag{80}$$

where $\mathbf{w} = [w_x, w_y]^T$ is a vector with test functions and $\mathbf{t} = [t_x, t_y]^T$ are the user-prescribed tractions on the Neumann part Γ_n of the boundary. Using the finite element discretisation mentioned above, Eq. (79) leads to

$$\int_\Omega \mathbf{B}_u^T\mathbf{C}\mathbf{B}_u \mathrm{d}\Omega\ \mathbf{d}^c \equiv \mathbf{K}\mathbf{d} = \mathbf{f} \tag{81}$$

which defines the stiffness matrix $\mathbf{K}$. Furthermore, the strain–displacement matrix $\mathbf{B}_u = \mathbf{L}\mathbf{N}_u$, whilst the force vector $\mathbf{f}$ collects the contributions of the body forces as well as the externally applied tractions.

The gradient activity is introduced by using the displacements of classical elasticity as input in either Eq. (14), Eq. (15) or Eq. (16) – finite element implementations of all three formats have been discussed by Askes et al. (2008b). The displacement-based Ru-Aifantis approach has been implemented and tested earlier by Tenek and Aifantis (2002) and was also extended for use in damage mechanics by Rodríguez-Ferran et al. (2005). We will treat the finite element discretisation of Eq. (16) in some detail; the discretisation of Eq. (14) or Eq. (15) is a straightforward exercise. The matrix–vector version of Eq. (16) reads

$$\mathbf{C}\left(\boldsymbol{\varepsilon}^g - \ell^2\nabla^2\boldsymbol{\varepsilon}^g\right) = \mathbf{C}\mathbf{L}\mathbf{u}^c \tag{82}$$

where $\boldsymbol{\varepsilon}^g = [\varepsilon^g_{xx}, \varepsilon^g_{yy}, \gamma^g_{xy}]^T$. Again, the weak form is taken and the second-order gradient term is integrated by parts, which gives

$$\int_\Omega \left[\mathbf{w}^T\mathbf{C}\boldsymbol{\varepsilon}^g + \ell^2\left(\frac{\partial\mathbf{w}^T}{\partial x}\mathbf{C}\frac{\partial\boldsymbol{\varepsilon}^g}{\partial x} + \frac{\partial\mathbf{w}^T}{\partial y}\mathbf{C}\frac{\partial\boldsymbol{\varepsilon}^g}{\partial y}\right)\right]\mathrm{d}\Omega - \oint_\Gamma \mathbf{w}^T\ell^2(\mathbf{n}\cdot\nabla\mathbf{C}\boldsymbol{\varepsilon}^g)\mathrm{d}\Gamma = \int_\Omega \mathbf{w}^T\mathbf{C}\mathbf{L}\mathbf{u}^c\mathrm{d}\Omega \tag{83}$$

where $\mathbf{n} = [n_x, n_y]^T$ contains the components of the normal vector to the boundary Γ, and $\mathbf{w}$ now contains three components. We will ignore the boundary term for now and discuss boundary conditions in Section 5.3.

For the discretisation it is necessary to expand the shape function matrix $\mathbf{N}$ given in Eq. (77) to accomodate all three nonlocal strain components, by which $\boldsymbol{\varepsilon}^g = \mathbf{N}_\varepsilon\mathbf{e}^g$ where $\mathbf{e}^g$ contains the components of the nodal nonlocal strains. The same shape functions $\mathbf{N}_\varepsilon$ are used to discretise the test function vector $\mathbf{w}$, while we again use $\mathbf{u}^c = \mathbf{N}_u\mathbf{d}^c$. The resulting system of equations reads (Askes et al., 2008b)

$$\int_\Omega \left[\mathbf{N}_\varepsilon^T\mathbf{C}\mathbf{N}_\varepsilon + \ell^2\left(\frac{\partial\mathbf{N}_\varepsilon^T}{\partial x}\mathbf{C}\frac{\partial\mathbf{N}_\varepsilon}{\partial x} + \frac{\partial\mathbf{N}_\varepsilon^T}{\partial y}\mathbf{C}\frac{\partial\mathbf{N}_\varepsilon}{\partial y}\right)\right]\mathrm{d}\Omega\ \mathbf{e}^g = \int_\Omega \mathbf{N}_\varepsilon^T\mathbf{C}\mathbf{B}_u\mathrm{d}\Omega\ \mathbf{d}^c \tag{84}$$

The shape functions $\mathbf{N}_\varepsilon$ can be chosen independently of $\mathbf{N}_u$; it then seems most convenient to use the same finite element mesh for Eqs. (81) and (84).

5.2.2. Acceleration gradients

The gradient elasticity format with inertia gradients is probably the most efficient format, since the gradient enrichment can be introduced without computational overhead. In matrix–vector notation, the equations of motion can be written as

$$\mathbf{L}^T\mathbf{C}\mathbf{L}\mathbf{u} + \mathbf{b} = \rho\left(\ddot{\mathbf{u}} - \ell^2\nabla^2\ddot{\mathbf{u}}\right) \tag{85}$$

The only difference with respect to classical elasticity is the higher-order inertia term, which does not impose additional requirements on the continuity of the interpolation, therefore finite element discretisation is straightforward. The weak form of Eq. (85), upon integration by parts, reads

$$\int_\Omega (\mathbf{L}\mathbf{w})^T\mathbf{C}\mathbf{L}\mathbf{u}\mathrm{d}\Omega + \int_\Omega \rho\left[\mathbf{w}^T\ddot{\mathbf{u}} + \ell^2\left(\frac{\partial\mathbf{w}^T}{\partial x}\frac{\partial\ddot{\mathbf{u}}}{\partial x} + \frac{\partial\mathbf{w}^T}{\partial y}\frac{\partial\ddot{\mathbf{u}}}{\partial y}\right)\right]\mathrm{d}\Omega = \int_\Omega \mathbf{w}^T\mathbf{b}\mathrm{d}\Omega + \int_{\Gamma_n}\mathbf{w}^T\mathbf{t}\mathrm{d}\Gamma \tag{86}$$

where the tractions $\mathbf{t}$ now also include inertia effects. The discretised system of equations is obtained as Fish et al. (2002b,a)

$$[\mathbf{M} + \ell^2\mathbf{H}]\ddot{\mathbf{d}} + \mathbf{K}\mathbf{d} = \mathbf{f} \tag{87}$$

where $\mathbf{K}$ and $\mathbf{f}$ are the same as in Eq. (81). The two contributions to the mass matrix are defined as

$$\mathbf{M} = \int_\Omega \rho\mathbf{N}_u^T\mathbf{N}_u\mathrm{d}\Omega \quad \text{and} \quad \mathbf{H} = \int_\Omega \rho\left(\frac{\partial\mathbf{N}_u^T}{\partial x}\frac{\partial\mathbf{N}_u}{\partial x} + \frac{\partial\mathbf{N}_u^T}{\partial y}\frac{\partial\mathbf{N}_u}{\partial y}\right)\mathrm{d}\Omega \tag{88}$$

The system of equations in expression (87) has the same dimension as in classical elasticity. For a solution in the time domain, a time integration algorithm (e.g. the Newmark scheme) must be selected. Guidelines on the choice of the element size and the time step size, relative to the internal length scale ℓ, were derived by Askes et al. (2008c).

5.2.3. Combined strain-acceleration gradients

The dynamically consistent format of gradient elasticity, written in matrix–vector notation, reads

$$\mathbf{L}^T\mathbf{C}\mathbf{L}\left(\mathbf{u}^g - \ell_s^2\nabla^2\mathbf{u}^g\right) = \rho\left(\ddot{\mathbf{u}}^g - \ell_d^2\nabla^2\ddot{\mathbf{u}}^g\right) \tag{89}$$

where the superscript g has been used to indicate gradient dependence. Since there are now two higher-order terms, the Ru-Aifantis theorem of Section 2.2.2 cannot be applied directly, except for the case $\ell_s = \ell_d$, which is non-dispersive (Askes et al., 2007; Gitman et al., 2007a). However, the fourth-order p.d.e. can be split into two sets of second-order p.d.e. with a similar manipulation, that is

$$\mathbf{u}^g - \ell_s^2\nabla^2\mathbf{u}^g \equiv \mathbf{u}^a \tag{90}$$

by which Eq. (89) becomes

$$\mathbf{L}^T\mathbf{C}\mathbf{L}\mathbf{u}^a = \rho\left(\ddot{\mathbf{u}}^g - \ell_d^2\nabla^2\ddot{\mathbf{u}}^g\right) \tag{91}$$

where $\mathbf{u}^a$ are (as yet unidentified) auxiliary displacements.

It has been shown that Eqs. (90) and (91) can be written as a set of coupled and symmetric second-order p.d.e. (Askes et al., 2007; Bennett and Askes, 2009). Furthermore, the two displacement fields $\mathbf{u}^g$ and $\mathbf{u}^a$ can be identified as the macroscopic displacements $\mathbf{u}^{\mathrm{M}}$ and the microscopic displacements $\mathbf{u}^{\mathrm{m}}$, respectively (Bennett et al., 2007). Thus, the simultaneous appearance of macroscopic and microscopic displacements in the equations re-introduces the multi-scale nature of gradient elasticity that was present in Mindlin's theory of elasticity with microstructure, given in Eqs. (1)–(3). The resulting equations are obtained as

$$\mathbf{L}^T\mathbf{C}\mathbf{L}\mathbf{u}^{\mathrm{m}} = \rho\left(\frac{\ell_d^2}{\ell_s^2}\,\ddot{\mathbf{u}}^{\mathrm{m}} - \frac{\ell_d^2-\ell_s^2}{\ell_s^2}\,\ddot{\mathbf{u}}^{\mathrm{M}}\right) \tag{92}$$

$$\rho\left(-\frac{\ell_d^2-\ell_s^2}{\ell_s^2}\,\ddot{\mathbf{u}}^{\mathrm{m}} + \frac{\ell_d^2-\ell_s^2}{\ell_s^2}\,\ddot{\mathbf{u}}^{\mathrm{M}} - (\ell_d^2-\ell_s^2)\nabla^2\ddot{\mathbf{u}}^{\mathrm{M}}\right) = 0 \tag{93}$$

Since both equations are now second-order in space, a standard $\mathcal{C}^0$ implementation can be used. The weak form of Eq. (92), upon integration by parts, reads

$$\begin{aligned} &-\int_\Omega (\mathbf{L}\mathbf{w})^T\mathbf{C}\mathbf{L}\mathbf{u}^{\mathrm{m}}\mathrm{d}\Omega + \int_\Omega \mathbf{w}^T\mathbf{b}\mathrm{d}\Omega + \int_{\Gamma_n}\mathbf{w}^T\mathbf{t}\mathrm{d}\Gamma \\ &\quad= \int_\Omega \mathbf{w}^T\rho\left(\frac{\ell_d^2}{\ell_s^2}\,\ddot{\mathbf{u}}^{\mathrm{m}} - \frac{\ell_d^2-\ell_s^2}{\ell_s^2}\,\ddot{\mathbf{u}}^{\mathrm{M}}\right)\mathrm{d}\Omega \end{aligned} \tag{94}$$

which involves the standard traction boundary conditions in their usual format. A similar treatment of Eq. (93) results in

$$\begin{aligned} &\int_\Omega \rho\left[\mathbf{v}^T\frac{\ell_d^2-\ell_s^2}{\ell_s^2}\left(-\ddot{\mathbf{u}}^{\mathrm{m}} + \ddot{\mathbf{u}}^{\mathrm{M}}\right) + (\ell_d^2-\ell_s^2)\left(\frac{\partial\mathbf{v}^T}{\partial x}\frac{\partial\ddot{\mathbf{u}}^{\mathrm{M}}}{\partial x} + \frac{\partial\mathbf{v}^T}{\partial y}\frac{\partial\ddot{\mathbf{u}}^{\mathrm{M}}}{\partial y}\right)\right]\mathrm{d}\Omega \\ &\quad - \oint_\Gamma \mathbf{v}^T\rho(\ell_d^2-\ell_s^2)(\mathbf{n}\cdot\nabla\ddot{\mathbf{u}}^{\mathrm{M}})\mathrm{d}\Gamma = 0 \end{aligned} \tag{95}$$

where $\mathbf{v}$ is a vector of test functions.

It is assumed that the same shape functions $\mathbf{N}_u$ are used for the two coupled displacement fields as well as for the associated test functions. Ignoring the boundary integral in Eq. (95), the system of discretised equations reads

$$\begin{bmatrix} \frac{\ell_d^2}{\ell_s^2}\mathbf{M} & -\frac{\ell_d^2-\ell_s^2}{\ell_s^2}\mathbf{M} \\ -\frac{\ell_d^2-\ell_s^2}{\ell_s^2}\mathbf{M} & \frac{\ell_d^2-\ell_s^2}{\ell_s^2}\mathbf{M} + (\ell_d^2-\ell_s^2)\mathbf{H} \end{bmatrix}\begin{bmatrix}\ddot{\mathbf{d}}^{\mathrm{m}}\\ \ddot{\mathbf{d}}^{\mathrm{M}}\end{bmatrix} + \begin{bmatrix}\mathbf{K} & 0\\ 0 & 0\end{bmatrix}\begin{bmatrix}\mathbf{d}^{\mathrm{m}}\\ \mathbf{d}^{\mathrm{M}}\end{bmatrix} = \begin{bmatrix}\mathbf{f}\\ 0\end{bmatrix} \tag{96}$$

where $\mathbf{f}$ and $\mathbf{K}$ are given in Eq. (81), whilst $\mathbf{M}$ and $\mathbf{H}$ are given in Eq. (88). For positive definite system matrices, it is required that $\ell_d > \ell_s$. Discretisation aspects of Eq. (96), such as element size and time step selection, are discussed by Bennett and Askes (2009).

5.3. Consistent boundary conditions

In the previous Section we have treated the finite element equations in some detail, but we have only cursorily dealt with the boundary conditions. In fact, the issue of boundary conditions in gradient elasticity has long been a topic of debate. Adopting the distinction given in Section 5.1, gradient elasticity appears either as a set of fourth-order equations with the displacements as the sole unknowns, or as a set of coupled second-order equations with the displacements and the components of another variable (stresses, micro-deformations) as unknowns. In the former case, the higher order of the governing equations means that higher-order boundary conditions must be formulated. In the latter case, additional boundary conditions accompany the auxiliary differential equations.

Some implicit agreement among the community seems to emerge in that most authors use higher-order boundary conditions that are proportional to the *second-order derivatives* (rather than first-order derivatives) of the displacement. Recent discussions on the issue of boundary conditions in gradient elasticity can be found in Shu et al. (1999), Polizzotto (2003), Askes and Metrikine (2005), Askes et al. (2008b,a), Kaplunov and Pichugin (2008), Andrianov et al. (2010b), Froiio et al. (2010) and the majority of these studies confirm observed trends to adopt second-order displacement derivatives. Reasons for this particular choice are based on energy arguments (Polizzotto, 2003), removal of singularities (Askes et al., 2008b), suppressing undesired boundary layer effects (Askes et al., 2008a) or simply implementational convenience (Askes and Aifantis, 2002). However, some researchers have focussed on the correspondence between the gradient elasticity theory and the related discrete model, and the most appropriate format of the gradient elasticity boundary conditions then depends on the nature of the boundary condition in the discrete model (Kaplunov and Pichugin, 2008; Andrianov et al., 2010b).

Here, we will discuss boundary conditions as they are obtained in their variationally consistent format in Section 5.2, and we will return to using index notation. Furthermore, we will compare the obtained boundary conditions with the variationally consistent boundary conditions that are associated with Eq. (7). The latter have been derived by Mindlin, and complicated expressions have been obtained whereby derivatives were split into normal and tangential components (Mindlin, 1964; Mindlin and Eshel, 1968). We will not provide detailed derivations of these boundary conditions, but they can be summarised as follows:

- Either the displacements or a conjugated stress tensor are prescribed on the boundary. This stress tensor is similar to the stress σ_{ij} given in Eq. (11) and it contains contributions proportional to the strains and the second spatial derivative of the strains. In case acceleration gradients are included as well, it also contains a contribution proportional to the second time derivative of the strains.
- Either the (normal component of the) derivative of the displacements or a conjugated higher-order stress tensor are prescribed on the boundary. This higher-order stress tensor is proportional to the *second-order derivative of the displacements.*

In discussing the variationally consistent boundary conditions of the finite element implementations of Section 5.2, an important criterium will be to which extent the boundary conditions of the simplified models coincide with the boundary conditions of the original Mindlin model.

Throughout, superimposed bars indicate prescribed values of the relevant variables.

5.3.1. Strain gradients

Using the Ru-Aifantis theorem of Section 2.2.2, the gradient elasticity format with strain gradients leads to two pairs of boundary conditions. The first set are the boundary conditions of classical elasticity related to Eq. (81), that is

$$\text{either} \quad u_i^c = \bar{u}_i^c \quad \text{or} \quad n_j \sigma_{ij}^c = t_i \tag{97}$$

which is consistent with the first set of boundary conditions of the Mindlin model.

For the second set of equations, various options are available as discussed in Section 2.2.2: the second set of equations can be expressed in terms of displacements, strains, or strains pre-multiplied with the constitutive coefficients:

- It was shown by Askes et al. (2008b) that not all singularities are removed from the strain field of a mode I fracture test in case the second set of equations is written in terms of *displacements*, therefore we will not consider this particular option.
- Expressing the second set of equations in terms of *strains* leads to a model whereby all singularities are removed from the strain field, but the behaviour at a bi-material interface differs qualitatively from the behaviour of Eq. (12), that is the model prior to the operator split. Namely, the use of Eq. (15) sets continuity of the gradient of *strain* over the interface, whereas with Eq. (12) continuity of the gradient of *stress* is obtained. This was illustrated for the one-dimensional case by Askes et al. (2008b). We will not consider this format of operator split further.
- When the second set of equations is written in terms of *strains pre-multiplied with the constitutive coefficients*, that is Eq. (16), the associated boundary conditions are

$$\text{either} \quad \varepsilon_{ij}^g = \bar{\varepsilon}_{ij}^g \quad \text{or} \quad n_m \ell^2 C_{ijkl} \varepsilon_{kl,m}^g = 0 \tag{98}$$

These particular boundary conditions approach those of the Mindlin model best: the higher-order essential boundary conditions are related to displacement derivatives (though not necessarily normal derivatives) and the higher-order natural boundary conditions are cast in terms of strain derivatives, similar to the higher-order stress tensor of the Mindlin model. The two models behave qualitatively the same, although some minor quantitative differences remain (Askes et al., 2008b).

This particular solution method of gradient elasticity with strain gradients consists of a set of uncoupled equations, the first of which are the equilibrium equations. The second set of equations renders nonlocal strains, and the associated nonlocal stresses are not necessarily equilibrated. This may lead to difficulties in interpretation, for instance at free boundaries. However, it is also possible to prescribe the components of the nonlocal strain ε_{ij}^g such that the relevant corresponding nonlocal stress components are zero on free boundaries. This has been suggested recently by Aifantis (2009c,b) and will be further illustrated in Section 6.1.3.

5.3.2. Acceleration gradients

The partial differential equations of gradient elasticity with acceleration gradients only are second-order in space, therefore only one set of boundary conditions must be applied, although the natural boundary conditions are extended compared to classical elasticity. In particular,

$$\text{either} \quad u_i = \bar{u}_i \quad \text{or} \quad n_j \sigma_{ij} = n_j \left(C_{ijkl} u_{k,l} + \rho \ell^2 \ddot{u}_{i,j} \right) = t_i \tag{99}$$

For finite element implementations, this means that no special measures need to be taken, since the right-hand-sides of both essential and natural boundary conditions are the same as in classical elasticity. This is reflected in Eq. (87).

5.3.3. Combined strain-acceleration gradients

The variationally consistent boundary conditions of the dynamically consistent gradient elasticity model, in its operator-split version, have been derived by the authors in Askes et al. (2007). They read

$$\text{either} \quad u_i^{\mathrm{m}} = \bar{u}_i^{\mathrm{m}} \quad \text{or} \quad n_j \sigma_{ij}^{\mathrm{st}} = n_j C_{ijkl} \varepsilon_{kl}^{\mathrm{m}} = t_i \tag{100}$$

$$\text{either} \quad u_i^{\mathrm{M}} = \bar{u}_i^{\mathrm{M}} \quad \text{or} \quad n_j \sigma_{ij}^{\mathrm{in}} = n_j \rho (\ell_d^2 - \ell_s^2) \ddot{u}_{i,j}^{\mathrm{M}} = 0 \tag{101}$$

The left-hand-sides of the natural boundary conditions can be interpreted as the projections of two stress tensors, whereby Eqs. (100) and (101) contain a stiffness-related stress and an inertia-related stress, respectively. Thus, a non-standard natural boundary condition in terms of a higher-order stress tensor is absent in this format of gradient elasticity.

In a one-dimensional example, it has been suggested to use tyings between the microscopic and macroscopic displacements, that is $u^{\mathrm{m}} = u^{\mathrm{M}}$, on the boundaries in order to emulate the effects of the non-standard natural boundary condition (Askes et al., 2008a); such a constraint was shown to eliminate boundary layers and would also ensure that the same volume change is predicted by microscopic and macroscopic displacements. In Section 6.1.4 we will investigate the effects of such tyings on the removal of singularities.

6. Applications and new results

Whereas the previous Sections were focussed on a systematic discussion of earlier results, in this Section we will present some new results. The advantages of gradient elasticity, compared to classical elasticity, are threefold: (i) with gradient elasticity the singularities can be avoided that typically appear in classical elasticity, (ii) the size-dependent mechanical response of heterogeneous materials can be captured with gradient elasticity, and (iii) dispersive wave propagation can be described by gradient elasticity. Wave dispersion has already been addressed in the comparison between the various models given in Section 2.5 (see also Askes et al. (2008a) and Papargyri-Beskou et al. (2009) for two recent comparative studies), and we will focus here on the removal of singularities and the description of size effects.

Throughout, in the numerical examples spatial discretisation is performed with four-noded bi-linear quadrilateral finite elements. In the dynamic examples the unconditionally stable constant average acceleration variant of the Newmark scheme is used for time integration.

6.1. Removal of singularities

In classical elasticity, singularities may appear where abrupt changes in the boundary conditions occur or at non-convex corners in the domain. Singularities can be avoided when gradient elasticity is used with appropriate boundary conditions, as has been demonstrated on many occasions, see for instance (Altan and Aifantis, 1992; Ru and Aifantis, 1993; Unger and Aifantis, 1995; Altan and Aifantis, 1997; Lazar and Maugin, 2005; Askes et al., 2008b; Askes and Gitman, 2009; Gitman et al., 2010). We will study the effects of gradient elasticity on singularities appearing where point loads are applied as well as at the tips of sharp cracks. We will also investigate the effect of boundary conditions in dynamically consistent gradient elasticity. However, for illustration we will first review a simple analytical procedure for mode III fracture.

6.1.1. Static mode III fracture – analytical solution

Many studies have been devoted to analytical solutions of mode III cracks in gradient elasticity. Altan and Aifantis (1992)

used Fourier transforms for a finite crack in an infinite medium, whereas Unger and Aifantis (1995) formulated a closed form solution for a semi-infinite crack in an infinite medium, although at one stage in their derivations the assumption of unstable strain gradients was made. Vardoulakis and coworkers studied finite mode III cracks in infinite gradient elastic media with additional surface energy terms; this extra term does not change the field equations but has an effect on the boundary conditions (Vardoulakis et al., 1996; Exadaktylos et al., 1996). In all these studies, the higher-order boundary conditions were taken proportional to the second-order derivative of the displacement, except (Unger and Aifantis, 1995) where the first-order derivative of the displacement was used. More recently, Georgiadis (2003) analysed semi-infinite cracks in an infinite medium using the Aifantis theory in statics (although not acknowledged as such) and the dynamically consistent theory in dynamics. The results in the latter work predict a stress singularity the sign of which is opposite to that of classical elasticity, which seems to be an undesirable feature of this solution.

In view of the Ru-Aifantis theorems discussed in Section 2.2.2, the pertinent governing equation for mode III is expressed in terms of the shear strains as

$$\varepsilon^g_{ij} - \ell^2 \varepsilon^g_{ij,kk} = \varepsilon^c_{ij} \tag{102}$$

i.e. an inhomogeneous diffusion equation for the gradient-enriched strain ε^g_{ij} where the classical strain ε^c_{ij} acts as a source term. From classical linear elastic fracture mechanics it is well known that the shear strains exhibit singularities at the crack tip. For a finite crack in an infinite medium, the two non-vanishing shear strains of classical elasticity are given by

$$\varepsilon^c_{13} = -\frac{K_{III}}{2G\sqrt{2\pi r}}\sin\frac{\theta}{2} \quad \text{and} \quad \varepsilon^c_{23} = \frac{K_{III}}{2G\sqrt{2\pi r}}\cos\frac{\theta}{2} \tag{103}$$

where the usual polar coordinates r and θ are adopted with origin at the crack tip, $K_{III} = \tau^\infty\sqrt{\pi a}$ is the stress intensity factor and G is the shear modulus. Furthermore, τ^∞ is the far-field antiplane shear stress and a is half the crack length. For ε^g_{23} we can write

$$\varepsilon^g_{23} = \frac{K_{III}}{2G\sqrt{2\pi}}\,\mathcal{E}(r)\cos\frac{\theta}{2} \tag{104}$$

If we substitute this expression into Eq. (102), we find that the unknown function $\mathcal{E}(r)$ must satisfy the following equation:

$$\left(1+\frac{\ell^2}{4r^2}\right)\mathcal{E} - \ell^2\left(\frac{\partial^2\mathcal{E}}{\partial r^2}+\frac{1}{r}\frac{\partial\mathcal{E}}{\partial r}\right) = \frac{1}{\sqrt{r}} \tag{105}$$

This leads to a general solution for $\mathcal{E}(r)$ as

$$\mathcal{E} = \frac{1}{\sqrt{r}}\left(1 + Ae^{-r/\ell} + Be^{r/\ell}\right) \tag{106}$$

Here, A and B are constants that can be determined via the boundary conditions, including those at infinity. We require the far-field shear strain to be finite, hence $B = 0$. Furthermore, we set $\varepsilon^g_{23} = 0$ for $r \to 0$, by which it follows that $A = -1$. Thus,

$$\varepsilon^g_{23} = \frac{K_{III}}{2G\sqrt{2\pi r}}\left(1 - e^{-r/\ell}\right)\cos\frac{\theta}{2} \tag{107}$$

which is finite for $r \to 0$. A similar result can be obtained for the other gradient-enriched shear strain ε^g_{13}.

Using appropriate boundary conditions is essential for the removal of singularities, as we will explore further below. Other boundary conditions, such as the ones used by Georgiadis (2003), may not result in similarly simple solutions or may even lead to stresses and strains with a singularity proportional to $r^{-3/2}$, i.e. stronger than classical elasticity where it is proportional to $r^{-1/2}$.

6.1.2. Static mode III fracture – numerical solutions

Next, we will use numerical finite element solutions to simulate the behaviour of mode III fracture. We will verify that crack tip and point load singularities can be avoided with gradient elasticity. In addition, we will study the performance of gradient elasticity in cases where the crack is positioned perpendicular to a bi-material interface. In such cases, the order of the singularity depends on the relative magnitude of the elastic constants of the two materials, with the more severe singularities appearing in case the crack is positioned in the *stiffer* material. In a recent study, it was shown that such singularities can be removed if gradient elasticity is used in a mode I fracture problem (Askes and Gitman, 2009); here, we will extend the analysis to mode III fracture. The studied geometry and boundary conditions are shown in Fig. 3, where by $L = 500$ mm and $F = 10$ N. For a mode III test the only required material parameter in classical elasticity is the shear modulus G; here, $G_1 = 10$ N/mm^2 and $G_2 = 1000$ N/mm^2. Furthermore, the internal length scale $\ell = 50$ mm in the simulations with gradient elasticity.

Fig. 4 shows surface plots of the shear strain components γ_{xz} and γ_{yz}, both obtained from classical elasticity and from gradient elasticity whereby the latter is obtained from the former via Eq. (84). For these results, the domain was discretised with 32×32 four-noded quadrilateral finite elements. It can be seen that the local strain field (obtained with classical elasticity, that is $\ell = 0$) is dominated by singularities which occur where the two point loads are applied as well as at the crack tip. These singularities are removed by the gradient enrichment – note for instance the different scaling of the vertical axes used on the left and the right of Fig. 4. In Fig. 5 the nonlocal strain components are plotted along the line $y = 0$ for different finite element meshes (ranging from 8×8 elements to 64×64 elements). It can be seen that both strain components converge to a unique solution if gradient elasticity is used.

A more quantitative understanding can be obtained by investigating the actual values of the strains at the positions where singularities occur in classical elasticity. In Table 1, values of the local and nonlocal shear strains are collected at the point where the load is applied. Based on the values from the four finite element meshes, we have also carried out a Richardson extrapolation. It can be seen that the two local strain components roughly double in value for every successive mesh refinement. Thus, they do not converge – or rather, they converge to infinity. Convergence to finite values is observed for the two nonlocal strain components. However, convergence is slow, which is due to the ratio of shear moduli of the two materials. With $G_1 < G_2$, the order of the singularity is larger than for the homogeneous case $G_1 = G_2$, which has an adverse influence on the convergence of the numerical gradient elasticity solutions. Conversely, taking $G_1 > G_2$ (so that the crack extends through the softer material) reduces the order of the singularity and leads to improved convergence of the numerical gradient elasticity solutions, see (Askes and Gitman, 2009).

6.1.3. Static mode I fracture

In the next example, we revisit and extend the mode I fracture problem presented earlier by Askes et al. (2008b) and shown in Fig. 6. The geometrical and material parameters are $L = 1$ mm, $E = 1000$ N/mm^2, $\nu = 0.25$ and $\ell = 0.1$ mm. Prescribed displacements $\bar{u} = 0.01$ mm imply a nominal vertical normal strain $\varepsilon_{yy} = 0.01$ if effects of the crack are excluded. For symmetry reasons, only the top-right quarter is modelled. In an earlier study, convergence upon mesh refinement was demonstrated (Askes et al., 2008b); here, we will demonstrate the effects of equilibrating the nonlocal stresses with externally applied tractions.

In Fig. 7 the three nonlocal stress components, obtained from $\sigma^g_{ij} = C_{ijkl}\varepsilon^g_{kl}$, are plotted. The top-right quarter is modelled with 16×16 bilinear quadrilateral finite elements. In the left column of Fig. 7, the boundary conditions accompanying Eq. (83) are taken

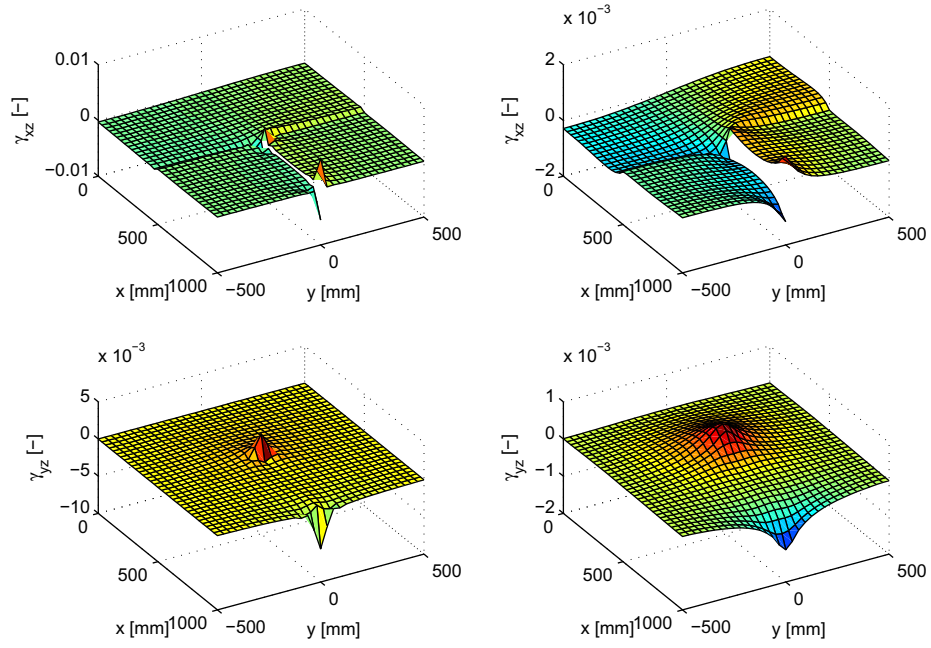

Fig. 4. Mode III fracture problem – surface plots of γ^c_{xz} (top left), γ^g_{xz} (top right), γ^c_{yz} (bottom left) and γ^g_{yz} (bottom right).

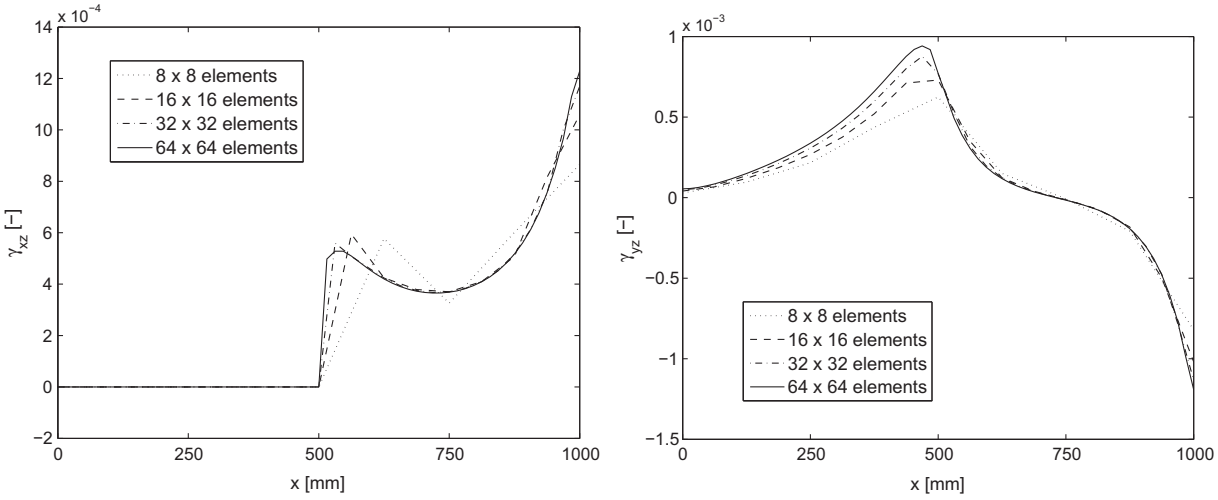

Fig. 5. Mode III fracture problem – convergence upon mesh refinement for γ^g_{xz} (left) and γ^g_{yz} (right) along $y = 0$.

Table 1
Mode III fracture problem – mesh refinement study and Richardson extrapolation for shear strains at position $(x,y) = (2L,0)$.

Mesh	γ^c_{xz}	γ^g_{xz}	γ^c_{yz}	γ^g_{yz}
8×8	$1.377 \cdot 10^{-3}$	$0.865 \cdot 10^{-3}$	$-1.372 \cdot 10^{-3}$	$-0.822 \cdot 10^{-3}$
16×16	$2.778 \cdot 10^{-3}$	$1.059 \cdot 10^{-3}$	$-2.765 \cdot 10^{-3}$	$-1.019 \cdot 10^{-3}$
32×32	$5.546 \cdot 10^{-3}$	$1.170 \cdot 10^{-3}$	$-5.539 \cdot 10^{-3}$	$-1.132 \cdot 10^{-3}$
64×64	$11.087 \cdot 10^{-3}$	$1.229 \cdot 10^{-3}$	$-11.083 \cdot 10^{-3}$	$-1.192 \cdot 10^{-3}$
Extrapolation	$20.785 \cdot 10^{-3}$	$1.290 \cdot 10^{-3}$	$-20.785 \cdot 10^{-3}$	$-1.254 \cdot 10^{-3}$

as *homogeneous natural boundary conditions* throughout, that is the natural boundary conditions suggested in Eq. (98). In the right column, the nonlocal strain components are prescribed such that $\sigma_{xx} = 0$ on the vertical edges, $\sigma_{yy} = 0$ on the face of the crack and $\sigma_{xy} = 0$ throughout. It can be seen that this particular adjustment of the boundary conditions has a moderate effect on the results. Although equilibrating the nonlocal stresses with externally applied tractions may facilitate interpretation of the results, it must be emphasised that the nonlocal stresses are not equilibrated inside the domain (i.e. away from the boundaries).

6.1.4. Point load singularities in dynamics

Next, we will study the removal, or otherwise, of singularities in dynamics. We will compare the gradient elasticity theory with acceleration gradients as well as the dynamically consistent theory with acceleration gradients and strain gradients. In order to separate the effects of field equations and boundary conditions, we consider the two problem statements given in Fig. 8. Singularities are expected in classical elasticity at the position where the point load is applied. In the geometry of Fig. 8(a), the singularity appears in the middle of the specimen and is therefore not influenced by boundary conditions. On the other hand, boundary conditions may affect the singularity in the geometry of Fig. 8(b) where the force is applied on the free boundary.

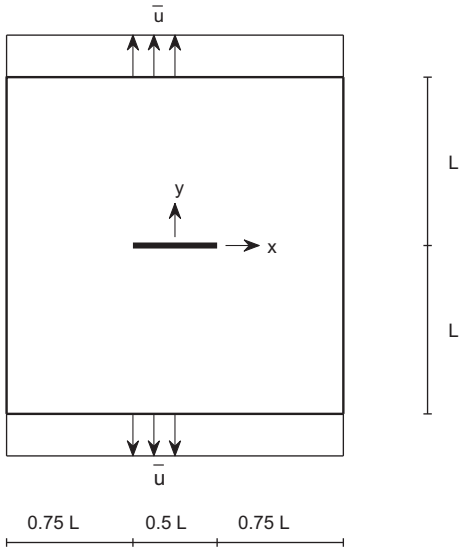

Fig. 6. Mode I fracture problem – geometry and boundary conditions; the solid line indicates the presence of a crack.

For the geometric and material parameters we have taken $H = 0.5$ m, $\rho = 1$ kg/m^3, and a plane strain assumption with $E = 100$ N/m^2 and $\nu = 0.25$. The length scale parameters are taken as $\ell = 0.1$ m in the model with acceleration gradients only, whereas $\ell_d = 0.1$ m and $\ell_s = 0.05$ m in the dynamically consistent model. The indicated forces are oriented 45° off the x-axis and they have magnitude $\sqrt{2}$ N; they are applied from time $t = 0$ s onwards. Sliding boundary conditions are applied where indicated in Fig. 8. Structured meshes are used with square finite elements of size h, and the number of elements is specified for the x-direction. For the time step Δt we follow the recommendations given by Bennett and Askes (2009) as $\Delta t = h\ell_d/2c_e\ell_s$. All reported results were obtained at time $t = 0.05$ s which is roughly equal to the time needed for the wave fronts to propagate to the edges of the indicated domains.

First, we study the performance of the model with acceleration gradients. In Fig. 9 the three strain components are plotted along the line $y = H$. The left and right column contain the results of Fig. 8(a) and (b), respectively. The various line types denote different mesh densities, ranging from 8 to 64 elements in the x-direction. Both columns of Fig. 9 show an unbounded growth of all three strain components, which indicate that singularities are present in the solution. From the results on the left of Fig. 9 it can be concluded that equipping the field equations with acceleration gradients is not sufficient to remove singularities. Furthermore, the results on the right of Fig. 9 demonstrate that this deficiency in the field equations cannot be ameliorated via the boundary conditions. Thus, this particular format of gradient elasticity is suitable to describe wave dispersion (as shown in Section 2.5) but not to remove singularities.

Secondly, the dynamically consistent gradient elasticity model is considered, in particular its multi-scale formulation discussed in Section 5.2.3. Fig. 10 shows the results pertaining to Fig. 8(a), whereby the two columns relate to the microscopic and macroscopic strains, whereby the various line types indicate different mesh densities again. Since the force is applied in the interior of the specimen, the format of the boundary conditions of this model as discussed in Section 5.3.3 is irrelevant for now. As can be seen from Fig. 10, singularities persist in the microscopic strain components (left column) but the macroscopic strain components (right column) are free of singularities; note the difference in vertical axis range. This can be understood as follows: from Eq. (90) it follows that

$$\varepsilon^{\mathrm{M}}_{ij} - \ell_s^2 \varepsilon^{\mathrm{M}}_{ij,kk} = \varepsilon^{\mathrm{m}}_{ij} \tag{108}$$

Comparing this last expression with Eqs. (9) and (10), we obtain by implication

$$\varepsilon^{\mathrm{M}}_{ij}(\mathbf{x}) = \int_V \alpha(\mathbf{s}) \varepsilon^{\mathrm{m}}_{ij}(\mathbf{x}+\mathbf{s}) \mathrm{d}V \tag{109}$$

which means that the macroscopic strain is the volume-average of the microscopic strain. Singularities in the microscopic strains do therefore not carry over to the macroscopic strains.

Next, the influence of boundary conditions in the multi-scale formulation of dynamically consistent gradient elasticity is studied. As discussed in Section 5.3.3, various options exist, in particular related to emulating the effect of zero higher-order stresses. In a one-dimensional study, it was suggested to apply tyings between macroscopic and microscopic displacement on the boundaries, i.e. add the constraint $u^{\mathrm{M}} = u^{\mathrm{m}}$ on the boundaries. This was shown to remove boundary layers from the macroscopic strain (Askes et al., 2008a). To extend this concept to multiple dimensions, one has the possibility to apply tyings to the normal components of the two displacement fields (i.e. require that $u^{\mathrm{M}}_i n_i = u^{\mathrm{m}}_i n_i$ where n_i are again the components of the outward normal vector) or to apply tyings to all displacement components (i.e. require that $u^{\mathrm{M}}_i = u^{\mathrm{m}}_i$). In Fig. 11 the strain components are plotted for the geometry of Fig. 8(b), using a finite element mesh of 32×16 elements. We have used the two variants of tyings described above, as well as leaving the macroscopic displacement unconstrained. The microscopic strains indicate singularities irrespective of which kind of boundary conditions is used for the macroscopic displacements. On the other hand, the boundary conditions have a significant effect on the macroscopic strain: leaving the macroscopic displacement unconstrained results in smooth macroscopic strains, whereas both types of tyings lead to singularities in all three macroscopic strain components. From these results, it seems that one has to accept the boundary layers reported in Askes et al. (2008a) for a complete removal of singularities from the macroscopic strains.

In summary, the following conclusions can be drawn regarding the removal of singularities in dynamics:

- Acceleration gradients alone do not remove singularities, irrespective of whether these appear in the interior of the domain or on the boundary. This indicates a deficiency in the field equations which cannot be remedied via appropriate boundary conditions.
- To remove singularities, it is a necessary (though not sufficient) condition that the field equations contain strain gradients.
- In the multi-scale formulation of dynamically consistent gradient elasticity, strain gradients can be effective to remove singularities from the macroscopic strains, although the associated microscopic strains are still singular.
- In the multi-scale formulation of dynamically consistent gradient elasticity, the boundary conditions play an important role in the removal of singularities. For all singularities to be removed from the macroscopic strains, the macroscopic displacement must remain unconstrained. Imposing tyings between macroscopic and microscopic displacement on the boundary may lead to singular macroscopic strains.

6.2. Size effect

Next, we will present some results on the size-dependent mechanical response of specimens modelled with gradient elasticity. The occurrence of size effects in gradient elasticity has been re-

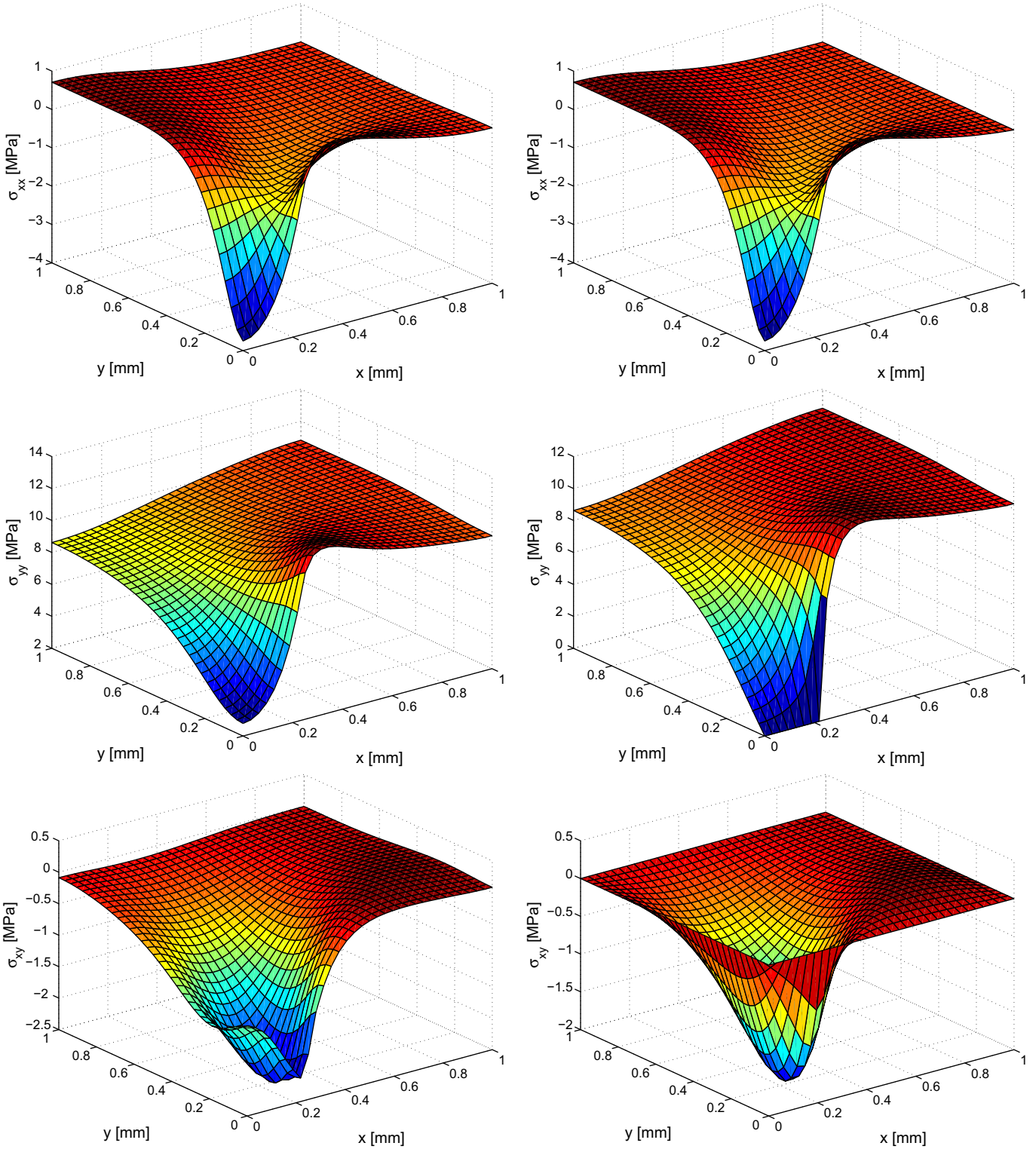

Fig. 7. Mode I fracture problem – surface plots of stress components σ^g_{xx} (top row), σ^g_{yy} (middle row) and σ_{xy} (bottom row); non-equilibrated (left column) and equilibrated (right column) on the boundaries.

ported before (Aifantis, 1995, 1999; Askes and Aifantis, 2002; Askes et al., 2008b). Here, we will study additional geometries that exhibit singularities in case classical elasticity is used. However, before we proceed with the presentation of new numerical results, we will discuss, as in the case of the elimination of elastic singularities, analytical results for a benchmark problem.

6.2.1. Shear layer

We consider an elastic layer of thickness H in the y-direction, extending infinitely far in the x-direction, subjected to an externally applied shear stress $\bar{\tau}$ parallel to the x-direction. In the absense of a body force, the governing one-dimensional equation reads

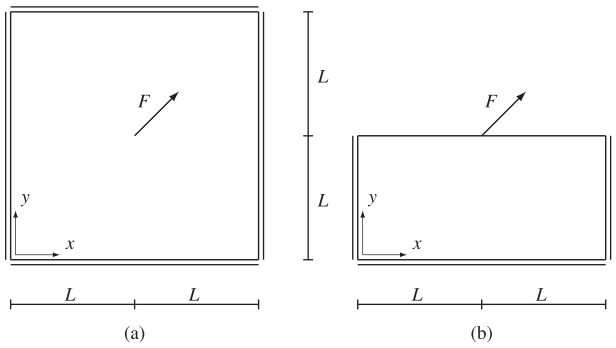

Fig. 8. Two geometries for dynamic analysis – force applied on interior of the domain (left) and on free boundary (right).

$$G\left(u_{x,yy} - \ell^2 u_{x,yyyy}\right) = 0 \tag{110}$$

The solution for u_y can be written as

$$u_x = A_1 + A_2 y + A_3 \sinh\left(\frac{y}{\ell}\right) + A_4 \cosh\left(\frac{y}{\ell}\right) \tag{111}$$

where the various A_i are constants that must be determined through the formulation of appropriate boundary conditions. We will adopt the following boundary conditions (Zervos, 2008):

$$y = 0: \quad u_x = 0 \tag{112}$$

$$y = \pm\frac{1}{2}H: \quad G\left(u_{x,y} - \ell^2 u_{x,yyy}\right) = \bar{\tau} \tag{113}$$

$$y = \pm\frac{1}{2}H: \quad u_{x,y} = 0 \tag{114}$$

After a bit of algebra, see Zervos (2008) for details, it is found that

$$u_x = \frac{\bar{\tau}}{G}\left(y - \ell\,\frac{\sinh(y/\ell)}{\cosh(H/2\ell)}\right) \tag{115}$$

and an effective (average) shear strain $\tilde{\gamma}$ as

$$\tilde{\gamma} \equiv \frac{1}{H}\int_{-\frac{1}{2}H}^{\frac{1}{2}H} \frac{\partial u_x}{\partial y}\,\mathrm{d}y = \frac{\bar{\tau}}{G}\left(1 - \frac{2\ell}{H}\tanh(H/2\ell)\right) \tag{116}$$

With an effective shear modulus $\tilde{G}$ defined as $\tilde{G} \equiv \bar{\tau}/\tilde{\gamma}$, the ratio of effective shear modulus over actual shear modulus is found as

$$\frac{\tilde{G}}{G} = \left(1 - \frac{2\ell}{H}\tanh(H/2\ell)\right)^{-1} \tag{117}$$

which is a decreasing function of H/ℓ. For relatively large specimens, where $\ell \ll H$, this ratio reaches the asymptotic value of 1, but larger values of effective stiffness are obtained for smaller specimens where ℓ is of the same order of magnitude as H.

Tekoglu and Onck (2005) simulated similar size effects in cellular materials. They used two modelling strategies: a detailed micro-structural model where every cell wall is included explicitly, as well as so-called *couple stress theory*. They studied the same shear layer problem that is discussed in this Section, and for this particular problem the governing equation of couple stress theory is identical to the governing equation of the 1992 Aifantis theory of gradient elasticity given in Eq. (110). Tekoglu and Onck fitted the response of couple stress theory with the response of the micro-structural model; they obtained an excellent agreement for the effective shear modulus, see (Tekoglu and Onck, 2005, Figs. 9 and 10). Since the governing equations for the shear layer problem are identical in couple stress theory and in gradient elasticity, it can be concluded that gradient elasticity is equally capable of fitting the size effects observed in the discrete modelling of cellular materials. The values of the length scale parameter ℓ can therefore be fitted to the cell size d of the cellular materials. For the regular and irregular hexagonal geometries studied by Tekoglu and Onck, the best fits are $\ell^2 \approx \frac{1}{32}d^2$ and $\ell^2 \approx \frac{1}{8}d^2$, respectively. This agrees quite well with the results of other studies that relate the length scale to the Representative Volume Size (Kouznetsova et al., 2004b; Gitman et al., 2004, 2005, 2007a) – as discussed in Section 4.1, all these studies suggest that $\ell^2 = \frac{1}{12}L_{\mathrm{RVE}}^2$.

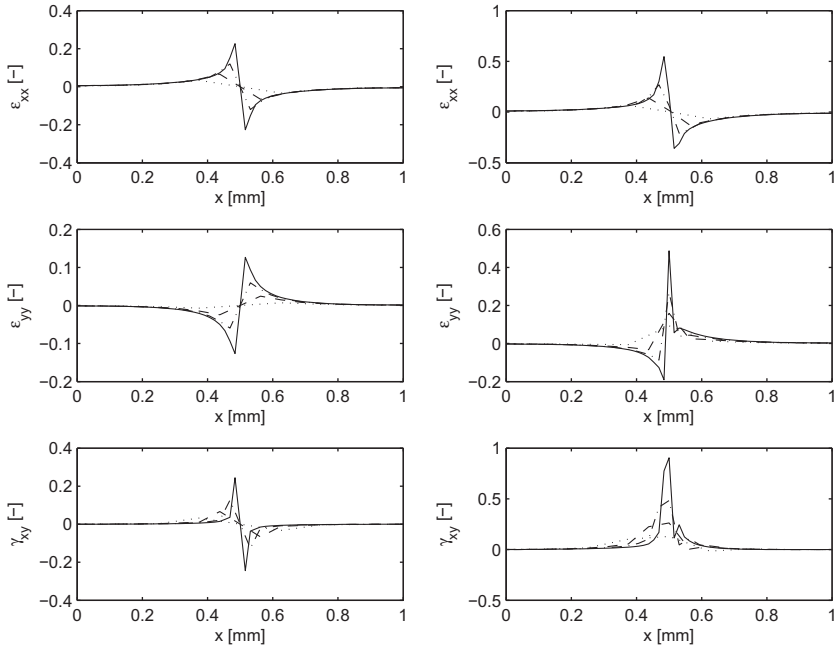

Fig. 9. Gradient elasticity with acceleration gradients – profiles of the strain components along the line $y = H$ for Fig. 8(a) in the left column and Fig. 8(b) in the right column. Line types indicate 8 (dotted), 16 (dashed), 32 (dash-dotted) and 64 (solid) elements in the x-direction.

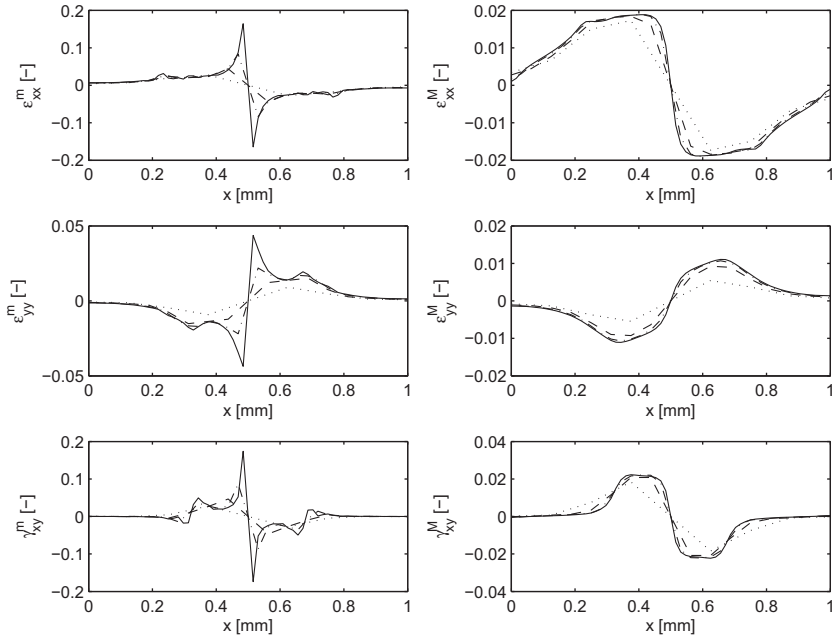

Fig. 10. Dynamically consistent gradient elasticity – profiles of microscopic strains (left) and macroscopic strains (right) along the line $y = H$ for Fig. 8(a). Line types indicate 8 (dotted), 16 (dashed), 32 (dash-dotted) and 64 (solid) elements in the x-direction.

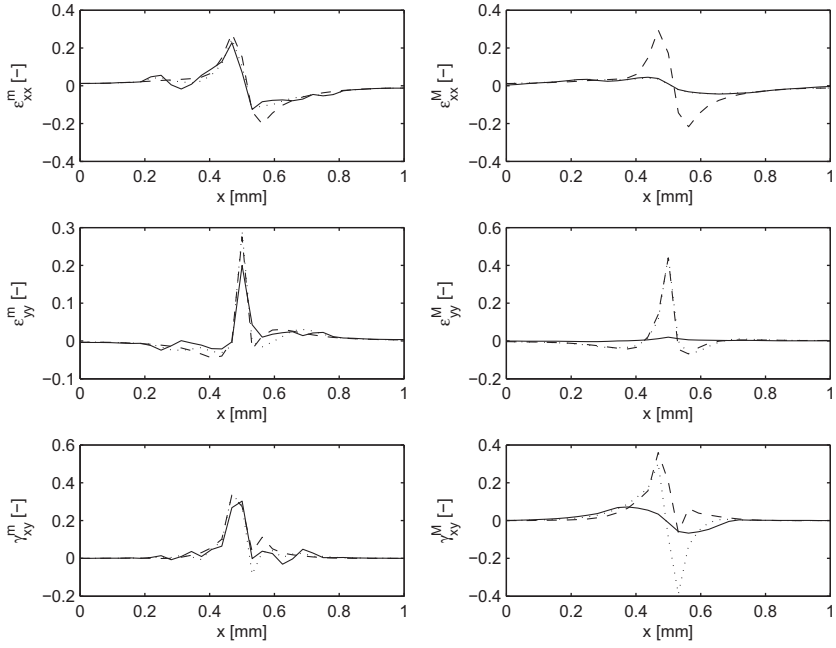

Fig. 11. Dynamically consistent gradient elasticity – profiles of microscopic strains (left) and macroscopic strains (right) along the line $y = H$ for Fig. 8(b). Line types indicate tying the normal displacement components on the boundary (dotted), tying both displacement components on the boundary (dashed), or leaving the macroscopic displacement unconstrained (solid).

Remark 11. Note that the definition of the length scale given by Tekoglu and Onck (2005) differs by a factor $\frac{1}{2}\sqrt{2}$ compared to the one used in Eq. (110); that is, the length scale ℓ_c used by Tekoglu and Onck is related to the length scale ℓ in Eq. (110) via $\ell^2 = \frac{1}{2}\ell_c^2$.

6.2.2. Square unit cell with square hole

The first numerical size effect example is the square unit cell with square hole as depicted in Fig. 12, which under the given boundary conditions can be thought of as the Representative Volume Element of a tensile plate with periodically spaced holes. The dimensions of the hole are related to the dimensions of the unit cell through a proportionality factor $\alpha = \frac{1}{4}$. The Young's modulus $E = 1000\ \mathrm{N/mm^2}$, the Poisson ratio $\nu = 0.25$ and the specimen is modelled with a plane stress assumption. The imposed displacement is scaled with the dimension L such that the nominal vertical normal strain $\varepsilon^{\mathrm{nom}}_{yy} \equiv \bar{u}/L = 0.01$, which leads to a nominal vertical normal stress $\sigma^{\mathrm{nom}}_{yy} = 10.67\ \mathrm{N/mm^2}$. The tested range of unit cell

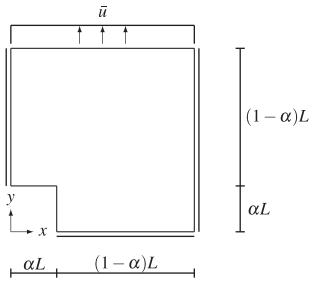

Fig. 12. Square unit cell with square hole – geometry and loading conditions.

dimensions is $L \in [0.25,0.5,1,2,4,8]$ mm. The material length scale parameter is taken as $\ell = 0.1$ mm. Following the recommendations for dynamics (Askes et al., 2008c; Bennett and Askes, 2009) the finite element size should be related to the magnitude of the length scale parameter. We have taken the element size roughly a third of the length scale parameter in the simulations with gradient elasticity. However, we have also carried out simulations with classical elasticity; we have distinguished here between analyses where the element size is constant (and equal to the analyses with gradient elasticity) and analyses where the element size scales proportionally with the geometric dimensions of the specimen.

We define a stress ratio as

$$\text{stress ratio} = \frac{\sigma_{yy}^{\text{nom}}}{\sigma_{yy}^{\max}} \tag{118}$$

where $\sigma_{yy}^{\max}$ is the vertical normal stress at the corner of the hole as retrieved from the finite element analysis. This stress ratio quantifies the stress concentration at the corner and is thus an indicator for the strength of the specimen: the lower the stress ratio, the lower one would expect the strength of the specimen to be. In Fig. 13 the stress ratio is plotted in a double-logarithmic scale against the specimen dimension L (normalised with the material length scale ℓ).

In classical elasticity, singularities are expected to appear at the corner of the hole where the stress is sampled. It then depends on the used finite element mesh (element size as well as polynomial degree of the shape functions) to what extend the singularity can be captured. If the element size is taken proportionally to the specimen dimension L, each finite element model is a perfectly scaled version of all other finite element models. As a consequence, the same stress distribution and the same stress ratio of Eq. (118) are expected. This is confirmed by the horizontal line in Fig. 13. On the other hand, if the finite element size is constant, irrespective of the size of the specimen, the larger specimens will have a relatively better resolution of the finite element mesh and thus provide a better approximation of the stress singularity. As a result, the stress ratio decreases with increasing specimen size if a constant element size is used.

In contrast, the singularities at the corner are removed when gradient elasticity is used. For the smaller specimen sizes, the material length scale ℓ is of the same order of magnitude as the dimension of the hole, and the result is an extreme smoothing of the stresses across the entire specimen. Therefore, the stress at the corner of the hole differs hardly from the nominal stress, and stress ratios very close to 1 are obtained. For the larger specimen sizes, there is some smoothing of the stresses through the gradient dependence, but a significant stress concentration is still present at the corner of the hole. Thus, stress ratios well below 1 are obtained.

6.2.3. Indentation

Next, we simulate an indentation test as shown in Fig. 14. A wedge-shaped indenter, assumed to be rigid, is pressed into a specimen of gradient-elastic material. The inclination angle of the indenter is set by a parameter α, and the interaction between the indenter and the gradient-elastic specimen is simulated with a simple contact algorithm. For symmetry reasons, only the right half of the problem is analysed. The prescribed displacement of the indenter is $\bar{u} = L/4\alpha$. The constitutive parameters of the gradient-elastic material are $E = 5000\ \text{N/mm}^2$, $\nu = \frac{1}{3}$ and $\ell = 0.1$ mm

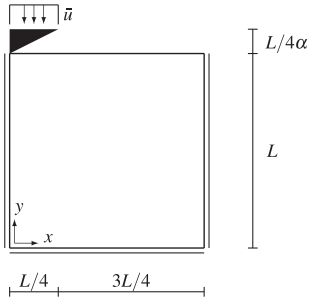

Fig. 14. Indentation test – geometry and loading conditions.

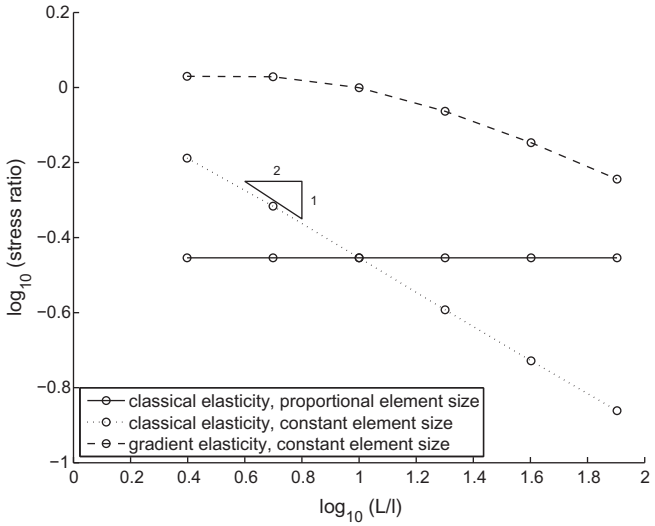

Fig. 13. Square unit cell with square hole – stress ratio versus specimen size for classical elasticity and gradient elasticity.

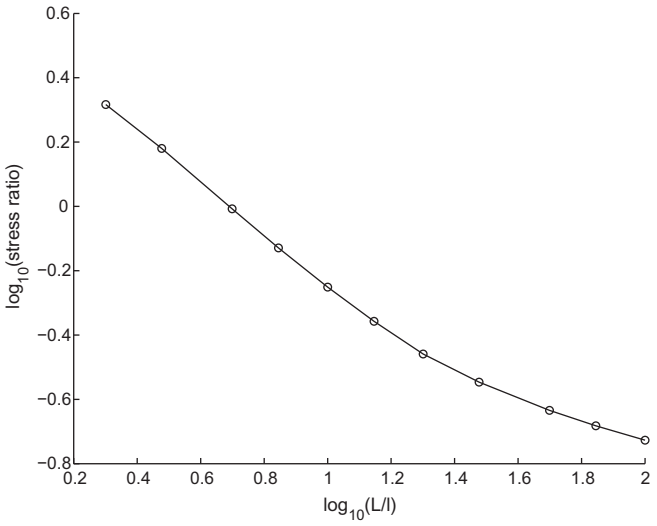

Fig. 15. Indentation test – stress ratio versus specimen size.

within a plane strain analysis. For the geometry, a range of specimen dimensions have been used ranging from $L = 0.2$ mm to $L = 10$ mm.

To obtain an indication for the strength of the specimen we use again Eq. (118), where now $\sigma_{yy}^{\text{nom}} = -E/4\alpha$ and $\sigma_{yy}^{\max}$ is evaluated at the tip of the indenter. In Fig. 15 we have plotted the stress ratio against the normalised specimen size. The curve has been obtained with $\alpha = 2$, but with the specific definition of the stress ratio the results are independent of the indenter's inclination angle. Firstly, it is noted that the stress ratio is finite, not singular as it would be in classical elasticity. For small values of L/ℓ the stress concentration at the indenter tip are smoothed significantly through the inclusion of strain gradients. For larger values of L/ℓ this effect of the strain gradients becomes less and less dominant.

7. Conclusions

In this paper, we have discussed various aspects of gradient elasticity. We have focussed on *Laplacian-based* gradient elasticity theories, that is, theories whereby the higher-order terms are proportional to the Laplacian of the corresponding lower-order terms. Furthermore, our emphasis has been mainly on *mono-scale* theories, whereby the kinematic variables relate to a single scale of observation. The higher-order terms may be strain gradients or acceleration gradients, which stem from additions to the potential energy density and kinetic energy density, respectively. The most important observations are summarised below.

- We have started our overview with Mindlin's theory of gradient elasticity. This particular model has five additional constitutive parameters associated with strain gradients and two associated with acceleration gradients, but in the Laplacien-format of the Mindlin theory the equations of motion have three independent length scales: two related to strain gradients (also referred to as stiffness-related length scales) and one related to acceleration gradients (i.e. an inertia-related length scale).
- For static applications, a single independent length scale seems enough. The most powerful reduction of the Mindlin model in statics is the 1992 Aifantis model, whereby the two length scales mentioned earlier are equal to each other. The Aifantis theory has been shown, on many occasions, to be effective in the removal of singularities and the description of size-dependent mechanical response. We do not claim that other simplifications of the Mindlin theory may not be equally effective; however, the 1992 Aifantis theory has the additional, and significant, advantage that finite element implementations are simple and straightforward.
- For dynamic applications, the inclusion of the inertia-related length scale is essential to describe dispersion. Without this term, phase velocities will either become unbounded or imaginary for the larger wave numbers. The inclusion of one or two independent stiffness-related length scales of the Mindlin model depends on the application. If the two stiffness-related length scales are equal to each other (as in the 1992 Aifantis theory), then the dispersion relations of compressive waves and shear waves are the same; if the two stiffness-related length scales are unequal the dispersion of compressive waves is quantitatively different from that of shear waves.
- The dynamically consistent format of gradient elasticity, which includes acceleration gradients as well as strain gradients, has also been shown to provide a unification of the two gradient elasticity theories of Eringen and Aifantis.
- There are still many attempts in the recent literature to model dynamic behaviour of microstructured materials with unstable gradient elasticity theories, e.g. (Yang and Guo, 2005; Wang and Hu, 2005; Every, 2005; Every et al., 2006; Wang et al., 2008; Maranganti and Sharma, 2007; Jakata and Every, 2008). Such theories are usually equipped with strain gradients but not with acceleration gradients. We have reviewed two studies from the recent literature where such gradient elasticity theories were used, and we have also suggested simple and straightforward improvements: the unstable strain gradients can be translated into stable stress gradients or stable acceleration gradients, without compromising the capacity to predict wave dispersion. In this paper, we advocate the use of acceleration gradients or, for greater flexibility, the combined use of acceleration gradients and (stable) strain gradients.
- The required identification and quantification of the additional constitutive parameters, usually cast as certain material length scale parameters, is normally perceived as a drawback of using gradient theories. We have provided an overview of analytical, numerical and experimental procedures by which the length scale parameters can be quantified or expressed in terms of other parameters that are more easily quantified.
- Another perceived drawback of using gradient elasticity theories is the lack of robust and efficient finite element implementations. However, much progress has been made in recent years. We have given an review of a number of approaches and treated in more detail certain formats of gradient elasticity that lend themselves to simple and efficient finite element implementations. In particular, the 1992 Aifantis theory of gradient elasticity, its operator split format due to Ru and Aifantis (1993) and its extension to dynamics (Askes and Aifantis, 2006; Askes et al., 2007) can be implemented efficiently using standard finite element technology.
- The removal of singularities from stress and strain fields has historically been one of the main motivations to use gradient elasticity. We have provided a few new results that demonstrate the importance of using appropriate boundary conditions. In statics, the Ru-Aifantis theorems can be applied on the level of displacements, strains or stresses, which lead to different variationally consistent boundary conditions. Singularities are avoided if the Ru-Aifantis theorem is applied to strains or stresses, see also (Askes et al., 2008b). In dynamics, we have used a multi-scale reformulation of dynamically consistent gradient elasticity, including strain gradients as well as acceleration gradients, and it was shown that it is essential to include strain gradients in order to avoid singularities – acceleration gradients alone are not sufficient. However, the boundary conditions also play an important role in the removal (or otherwise) of singularities.
- In contrast to classical elasticity, it is possible to simulate size-dependent mechanical behaviour with gradient elasticity. This has been demonstrated for a number of geometries, and in correspondence with earlier results from the literature it has been found that the gradient effects are most significant if the material length scale parameter is of the same order of magnitude as the dimension of the geometric object (hole, indentor or otherwise) that triggers gradient activity.

Acknowledgements

We gratefully acknowledge financial support of the European Commission (Grant No. 21069, "Deformation and fracture instabilities in novel materials and processes") and the Engineering and Physical Sciences Research Council (Grant No. EP/D041368/1) for financial support. We are also indebted to Pradeep Sharma, the lead author of Maranganti and Sharma (2007), for the many fruitful discussions and constructive comments on Section 3.1.

References

Aero, E., Kuvshinskii, E., 1961. Fundamental equations of the theory of elastic media with rotationally interacting particles. Soviet Phys. – Solid State 2, 1272–1281.

Aifantis, E., 1984. On the microstructural origin of certain inelastic models. ASME J. Eng. Mater. Technol. 106, 326–330.

Aifantis, E., 1987. The physics of plastic deformation. Int. J. Plast. 3, 211–247.

Aifantis, E., 1992. On the role of gradients in the localization of deformation and fracture. Int. J. Eng. Sci. 30, 1279–1299.

Aifantis, E., 1995. Higher order gradients and size effects. In: Carpinteri, A. (Ed.), Size-Scale Effects in the Failure Mechanisms of Materials and Structures. Routledge, pp. 231–242.

Aifantis, E., 1999. Strain gradient interpretation of size effects. Int. J. Fract. 95, 299–314.

Aifantis, E., 2000. Nanomechanics: an introduction. In: Katsikadelis, T., Beskos, D., Gdoutos, E. (Eds.), Recent Adv. Appl. Mech. (Honorary Volume for Academician A.N. Kounadis). pp. 243–254.

Aifantis, E., 2003. Update on a class of gradient theories. Mech. Mat. 35, 259–280.

Aifantis, E., 2009a. Exploring the applicability of gradient elasticity to certain micro/nano reliability problems. Microsyst. Technol. 15, 109–115.

Aifantis, E., 2009b. On scale invariance in anisotropic plasticity, gradient plasticity and gradient elasticity. Int. J. Eng. Sci. 47, 1089–1099.

Aifantis, E., 2009c. On stress concentrators and the elimination of elastic singularities: a gradient approach. In: 2009 SEM Annual Conference on Experimental and Applied Mechanics.

Altan, S., Aifantis, E., 1992. On the structure of the mode III crack-tip in gradient elasticity. Scripta Metall. Mater. 26, 319–324.

Altan, B., Aifantis, E., 1997. On some aspects in the special theory of gradient elasticity. J. Mech. Behav. Mat. 8, 231–282.

Amanatidou, E., Aravas, N., 2002. Mixed finite element formulations of strain-gradient elasticity problems. Comput. Methods Appl. Mech. Eng. 191, 1723–1751.

Andrianov, I., Awrejcewicz, J., 2008. Continuous models for 2D discrete media valid for higher-frequency domain. Comput. Struct. 86, 140–144.

Andrianov, I., Awrejcewicz, J., Barantsev, R., 2003. Asymptotic approaches in mechanics: new parameters and procedures. ASME Appl. Mech. Rev. 56, 87–110.

Andrianov, I., Bolshakov, V., Danishevskyy, V., Weichert, D., 2008. Higher order asymptotic homogenization and wave propagation in periodic composite materials. Proc. Roy. Soc. A 464, 1181–1201.

Andrianov, I., Awrejcewicz, J., Danishevskyy, V., Weichert, D., 2010a. Wave propagation in periodic composites: Higher-order asymptotic analysis versus plane-wave expansions method. ASME J. Comput. Nonlinear Dyn. 6, 011015.

Andrianov, I., Awrejcewicz, J., Weichert, D., 2010b. Improved continuous models for discrete media. Math. Probl. Eng., 986242.

Arnold, D., Winther, R., 2002. Mixed finite elements for elasticity. Numer. Math. 92, 401–419.

Arnold, D., Douglas Jr., J., Gupta, C., 1984. A family of higher-order mixed finite element methods for plane elasticity. Numer. Math. 45, 1–22.

Askes, H., Aifantis, E., 2002. Numerical modeling of size effect with gradient elasticity – formulation, meshless discretization and examples. Int. J. Fract. 117, 347–358.

Askes, H., Aifantis, E., 2006. Gradient elasticity theories in statics and dynamics – a unification of approaches. Int. J. Fract. 139, 297–304.

Askes, H., Aifantis, E., 2009. Gradient elasticity and flexural wave dispersion in carbon nanotubes. Phys. Rev. B 80, 195412.

Askes, H., Gitman, I., 2009. Non-singular stresses in gradient elasticity at bi-material interface with transverse crack. Int. J. Fract. 156, 217–222.

Askes, H., Gitman, I., 2010. Review and critique of the stress gradient elasticity theories of Eringen and Aifantis. In: Maugin, G., Metrikine, A. (Eds.), Mechanics of Generalized Continua. Springer, pp. 203–210.

Askes, H., Gutiérrez, M., 2006. Implicit gradient elasticity. Int. J. Numer. Meth. Eng. 67, 400–416.

Askes, H., Metrikine, A., 2002. One-dimensional dynamically consistent gradient elasticity models derived from a discrete microstructure. Part 2: static and dynamic response. Eur. J. Mech. A/Solids 21, 573–588.

Askes, H., Metrikine, A., 2005. Higher-order continua derived from discrete media: continualisation aspects and boundary conditions. Int. J. Solids Struct. 42, 187–202.

Askes, H., Suiker, A., Sluys, L., 2002. A classification of higher-order strain gradient models – linear analysis. Arch. Appl. Mech. 72, 171–188.

Askes, H., Bennett, T., Aifantis, E., 2007. A new formulation and C^0-implementation of dynamically consistent gradient elasticity. Int. J. Numer. Meth. Eng. 72, 111–126.

Askes, H., Metrikine, A., Pichugin, A., Bennett, T., 2008a. Four simplified gradient elasticity models for the simulation of dispersive wave propagation. Phil. Mag. 88, 3415–3443.

Askes, H., Morata, I., Aifantis, E., 2008b. Finite element analysis with staggered gradient elasticity. Comput. Struct. 86, 1266–1279.

Askes, H., Wang, B., Bennett, T., 2008c. Element size and time step selection procedures for the numerical analysis of elasticity with higher-order inertia. J. Sound Vibr. 314, 650–656.

Bennett, T., Askes, H., 2009. Finite element modelling of wave dispersion with dynamically consistent gradient elasticity. Comput. Mech. 43, 815–825.

Bennett, T., Gitman, I., Askes, H., 2007. Elasticity theories with higher-order gradients of inertia and stiffness for the modelling of wave dispersion in laminates. Int. J. Fract. 148, 185–193.

Carstensen, C., Günther, D., Reininghaus, J., Thiele, J., 2008. The Arnold-Winther mixed FEM in linear elasticity. Part I: implementation and numerical verification. Comput. Meth. Appl. Mech. Eng. 197, 3014–3023.

Cauchy, A., 1850a. Mémoire sur les systèmes isotropes de points matériels. In: Oeuvres complètes, 1re Série – Tome II. Gauthier-Villars (reprint 1908), Paris, pp. 351–386.

Cauchy, A., 1850b. Mémoire sur les vibrations d'un double système de molécules et de l'éther continu dans un corps cristallisé. In: Oeuvres complètes, 1re Série – Tome II. Gauthier-Villars (reprint 1908), Paris, pp. 338–350.

Cauchy, A., 1851. Note sur l'équilibre et les mouvements vibratoires des corps solides. In: Oeuvres complètes, 1re Série – Tome XI. Gauthier-Villars (reprint 1899), Paris, pp. 341–346.

Chang, C., Gao, J., 1995. Second-gradient constitutive theory for granular material with random packing structure. Int. J. Solids Struct. 32, 2279–2293.

Chen, W., Fish, J., 2001. A dispersive model for wave propagation in periodic heterogeneous media based on homogenization with multiple spatial and temporal scales. ASME J. Appl. Mech. 68, 153–161.

Cirak, F., Ortiz, M., Schröder, P., 2000. Subdivision surfaces: a new paradigm for thin-shell finite-element analysis. Int. J. Numer. Methods Eng. 47, 2039–2072.

Collins, M., 1981. A quasicontinuum approximation for solitons in an atomic chain. Chem. Phys. Lett. 77, 342–347.

Comi, C., 1999. Computational modelling of gradient-enhanced damage in quasi-brittle materials. Mech. Coh.-Frict. Mater. 4, 17–36.

Cosserat, E., Cosserat, F., 1909. Théorie des corps déformables. Hermann Archives (reprint 2009).

de Borst, R., Mühlhaus, H.-B., 1992. Gradient-dependent plasticity: formulation and algorithmic aspects. Int. J. Numer. Methods Eng. 35, 521–539.

de Borst, R., Pamin, J., Peerlings, R., Sluys, L., 1995. On gradient-enhanced damage and plasticity models for failure in quasi-brittle and frictional materials. Comput. Mech. 17, 130–141.

DiVicenzo, D., 1986. Dispersive corrections to continuum elastic theory in cubic crystals. Phys. Rev. B 34, 5450–5465.

Duan, W., Wang, C., Zhang, Y., 2007. Calibration of nonlocal scaling effect parameter for free vibration of carbon nanotubes by molecular dynamics. J. Appl. Phys. 101, 024305.

Engelbrecht, J., Berezovski, A., Pastrone, F., Braun, M., 2005. Waves in microstructured materials and dispersion. Phil. Mag. 85, 4127–4141.

Engel, G., Garikipati, K., Hughes, T., Larson, M., Mazzei, L., Taylor, R., 2002. Continuous/discontinuous finite element approximations of fourth-order elliptic problems in structural and continuum mechanics with applications to thin beams and plates, and strain gradient elasticity. Comput. Methods Appl. Mech. Eng. 191, 3669–3750.

Eringen, A., 1983. On differential equations of nonlocal elasticity and solutions of screw dislocation and surface waves. J. Appl. Phys. 54, 4703–4710.

Erofeyev, V., 2003. Wave Processes in Solids with Microstructure. World Scientific.

Every, A., 2005. Weak spatial dispersion and the unfolding of wave arrival singularities in the elastodynamic Greens functions of solids. Phys. Rev. B 72, 104302.

Every, A., Kaplunov, J., Rogerson, G., 2006. Unfolding of wave-arrival singularities in the elastodynamic Greens functions of anisotropic solids under weak spatial dispersion. Phys. Rev. B 74, 184307.

Exadaktylos, G., Vardoulakis, I., Aifantis, E., 1996. Cracks in gradient elastic bodies with surface energy. Int. J. Fract. 79, 107–119.

Fish, J., Chen, W., Nagai, G., 2002a. Non-local dispersive model for wave propagation in heterogeneous media: multi-dimensional case. Int. J. Numer. Methods Eng. 54, 347–363.

Fish, J., Chen, W., Nagai, G., 2002b. Non-local dispersive model for wave propagation in heterogeneous media: one-dimensional case. Int. J. Numer. Methods Eng. 54, 331–346.

Frantziskonis, G., Aifantis, E., 2002. On the stochastic interpretation of gradient-dependent constitutive equations. Eur. J. Mech. A/Solids 21, 589–596.

Fremond, M., Nedjar, B., 1996. Damage, gradient of damage and principle of virtual power. Int. J. Solids Struct. 33, 1083–1103.

Froiio, F., Zervos, A., Vardoulakis, I., 2010. On natural boundary conditions in linear 2nd-grade elasticity. In: Maugin, G., Metrikine, A. (Eds.), Mechanics of Generalized Continua. Springer, pp. 211–221.

Georgiadis, H., 2003. The mode III crack problem in microstructured solids governed by dipolar gradient elasticity: static and dynamic analysis. ASME J. Appl. Mech. 70, 517–530.

Georgiadis, H., Anagnostou, D., 2008. Problems of the Flamant-Boussinesq and Kelvin type in dipolar gradient elasticity. J. Elast. 90, 71–98.

Georgiadis, H., Vardoulakis, I., Lykotrafitis, G., 2000. Torsional surface waves in a gradient-elastic half-space. Wave Mot. 31, 333–348.

Gitman, I., Askes, H., Sluys, L., 2004. Representative Volume size as a macroscopic length scale parameter. In: Li, V.C. et al. (Ed.), Fract. Mech. Concr. Struct. IaFraMCoS, pp. 483–489.

Gitman, I., Askes, H., Aifantis, E., 2005. The representative volume size in static and dynamic micro-macro transitions. Int. J. Fract. 135, L3–L9.

Gitman, I., Gitman, M., Askes, H., 2006. Quantification of stochastically stable representative volumes for random heterogeneous materials. Arch. Appl. Mech. 75, 79–92.

Gitman, I., Askes, H., Aifantis, E., 2007a. Gradient elasticity with internal length and internal inertia based on the homogenisation of a representative volume element. J. Mech. Behav. Mater. 18, 1–16.

Gitman, I., Askes, H., Sluys, L., 2007b. Representative volume: existence and size determination. Eng. Fract. Mech. 74, 2518–2534.

Gitman, I., Askes, H., Sluys, L., 2008. Coupled-volume multi-scale modelling of quasibrittle material. Eur. J. Mech. A/Solids 27, 302–327.

Gitman, I., Askes, H., Kuhl, E., Aifantis, E., 2010. Stress concentrations in fractured compact bone simulated with a special class of anisotropic gradient elasticity. Int. J. Solids Struct. 47, 1099–1107.

Green, A., Rivlin, R., 1964a. Multipolar continuum mechanics. Arch. Rat. Mech. Anal. 17, 113–147.

Green, A., Rivlin, R., 1964b. Simple force and stress multipoles. Arch. Rat. Mech. Anal. 16, 325–353.

Gutkin, M., 2000. Nanoscopics of dislocations and disclinations in gradient elasticity. Rev. Adv. Mater. Sci. 1, 27–60. available via <http://www.ipme.ru>.

Gutkin, M., Aifantis, E., 1996. Screw dislocation in gradient elasticity. Scripta Mater. 35, 1353–1358.

Gutkin, M., Aifantis, E., 1997. Edge dislocation in gradient elasticity. Scripta Mater. 36, 129–135.

Gutkin, M., Aifantis, E., 1999. Dislocations in the theory of gradient elasticity. Scripta Mater. 40, 559–566.

Huerta, A., Pijaudier-Cabot, G., 1994. Discretization influence on the regularization by two localization limiters. ASCE J. Eng. Mech. 120, 1198–1218.

Ioannidou, T., Pouget, J., Aifantis, E., 2001. Kink dynamics in a lattice model with long-range interactions. J. Phys. A – Math. Gen. 34, 4269–4280.

Jakata, K., Every, A., 2008. Determination of the dispersive elastic constants of the cubic crystals Ge, Si, GaAs, and InSb. Phys. Rev. B. 77, 174301.

Kanit, T., Forest, S., Galliet, I., Mounoury, V., Jeulin, D., 2003. Determination of the size of the representative volume element for random composites: statistical and numerical approach. Int. J. Solids Struct. 40, 3647–3679.

Kaplunov, J., Pichugin, A., 2008. On rational boundary conditions for higher-order long-wave models. In: Borodich, F. (Ed.), IUTAM Symposium on Scaling in Solid Mechanics. Springer, pp. 81–90.

Karlis, G., Tsinopoulos, S., Polyzos, D., Beskos, D., 2007. Boundary element analysis of mode I and mixed mode (I and II) crack problems of 2-D gradient elasticity. Comput. Methods Appl. Mech. Eng. 196, 5092–5103.

Kioseoglou, J., Dimitrakopulos, G., Komninou, P., Karakostas, T., Konstantopoulos, I., Avlonitis, M., Aifantis, E., 2006. Analysis of partial dislocations in wurtzite GaN using gradient elasticity. Phys. Stat. Sol. A – Appl. Mat. Sci. 203, 2161–2166.

Kioseoglou, J., Dimitrakopulos, G., Komninou, P., Karakostas, T., Aifantis, E., 2008. Dislocation core investigation by geometric phase analysis and the dislocation density tensor. J. Phys. D – Appl. Phys. 41, 035408.

Kioseoglou, J., Konstantopoulos, I., Ribarik, G., Dimitrakopulos, G., Aifantis, E., 2009. Nonsingular dislocation and crack fields: implications to small volumes. Microsyst. Technol. 15, 117–121.

Kouznetsova, V., Geers, M., Brekelmans, W., 2002. Multi-scale constitutive modelling of heterogeneous materials with a gradient-enhanced computational homogenization scheme. Int. J. Numer. Methods Eng. 54, 1235–1260.

Kouznetsova, V., Geers, M., Brekelmans, W., 2004a. Multi-scale second-order computational homogenization of multi-phase materials: a nested finite element solution strategy. Comput. Methods Appl. Mech. Eng. 193, 5525–5550.

Kouznetsova, V., Geers, M., Brekelmans, W., 2004b. Size of a representative volume element in a second-order computational homogenization framework. Int. J. Multiscale Comput. Eng. 2, 575–598.

Kröner, E., 1963. On the physical reality of torque stresses in continuum mechanics. Int. J. Eng. Sci. 1, 261–278.

Kröner, E., 1967. Elasticity theory of materials with long range cohesive forces. Int. J. Sol. Struct. 3, 731–742.

Kunin, I., 1966. Theory of elasticity with spatial dispersion. One-dimensional complex structure. J. Appl. Math. Mech. 30, 1025–1034.

Lam, D., Yang, F., Chong, A., Wang, J., Tong, P., 2003. Experiments and theory in strain gradient elasticity. J. Mech. Phys. Solids 51, 1477–1508.

Lazar, M., Maugin, G., 2005. Nonsingular stress and strain fields of dislocations and diclinations in first strain gradient elasticity. Int. J. Eng. Sci. 43, 1157–1184.

Levin, V., 1971. The relation between mathematical expectations of stress and strain tensors in elastic microheterogeneous media. J. Appl. Math. Mech. 35, 694–701.

Lurie, S., Belov, P., Volkov-Bogorodsky, D., Tuchkova, N., 2003. Nanomechanical modeling of nanostructures and dispersed composites. Comput. Mater. Sci. 28, 529–539.

Maranganti, R., Sharma, P., 2007. A novel atomistic approach to determine strain-gradient elasticity constants: tabulation and comparison for various metals, semiconductors, silica, polymers and the (ir)relevance for nanotechnologies. J. Mech. Phys. Sol. 55, 1823–1852.

Matsushima, T., Chambon, R., Caillerie, D., 2002. Large strain finite element analysis of a local second gradient model: application to localization. Int. J. Numer. Methods Eng. 54, 499–521.

Metrikine, A., 2006. On causality of the gradient elasticity models. J. Sound Vibr. 297, 727–742.

Metrikine, A., Askes, H., 2002. One-dimensional dynamically consistent gradient elasticity models derived from a discrete microstructure. Part 1: Generic formulation. Eur. J. Mech. A/Solids 21, 555–572.

Metrikine, A., Askes, H., 2006. An isotropic dynamically consistent gradient elasticity model derived from a 2D lattice. Phil. Mag. 86, 3259–3286.

Metrikine, A., Prokhorova, J., 2010. On the uniqueness of the Lagrangian of gradient elastic continua. In: Maugin, G., Metrikine, A. (Eds.), Mechanics of Generalized Continua. Springer, pp. 149–160.

Mindlin, R., 1964. Micro-structure in linear elasticity. Arch. Rat. Mech. Anal. 16, 52–78.

Mindlin, R., 1965. Second gradient of strain and surface-tension in linear elasticity. Int. J. Solids Struct. 1, 417–438.

Mindlin, R., 1968. Theories of elastic continua and crystal lattice theories. In: Kroner, E. (Ed.), IUTAM Symposium Mechanics of Generalized Continua. Springer-Verlag, Berlin, pp. 312–320.

Mindlin, R., Eshel, N., 1968. On first strain-gradient theories in linear elasticity. Int. J. Solids Struct. 4, 109–124.

Mindlin, R., Tiersten, H., 1962. Effects of couple-stresses in linear elasticity. Arch. Rat. Mech. Anal. 11, 415–448.

Morgan, A., 1966. Some properties of media defined by constitutive equations in implicit form. Int. J. Eng. Sci. 4, 155–178.

Mühlhaus, H.-B., Oka, F., 1996. Dispersion and wave propagation in discrete and continuous models for granular materials. Int. J. Solids Struct. 33, 2841–2858.

Opie, A., Grindlay, J., 1972. Calculation of the coefficients describing the linear dependence of the stress tensor on the second order material gradients of the displacement gradients: rare gas solids. J. Phys. C: Solid State Phys. 5, 3289–3295.

Ostoja-Starzewski, M., 2002. Microstructural randomness versus representative volume element in thermomechanics. ASME J. Appl. Mech. 69, 25–35.

Özkirimli, U., Sofos, S., 2008. Tormented by history – Nationalism in Greece and Turkey. Hurst.

Pal'mov, V., 1964. Fundamental equations of the theory of asymmetric elasticity. J. Appl. Math. Mech. 28, 496–505.

Papanicolopulos, S.-A., Zervos, A., Vardoulakis, I., 2009. A three-dimensional C^1 finite element for gradient elasticity. Int. J. Numer. Methods Eng. 77, 1396–1415.

Papargyri-Beskou, S., Polyzos, D., Beskos, D., 2009. Wave dispersion in gradient elastic solids and structures: a unified treatment. Int. J. Solids Struct. 46, 3751–3759.

Peerlings, R., de Borst, R., Brekelmans, W., de Vree, J., 1996a. Gradient enhanced damage for quasi-brittle materials. Int. J. Numer. Methods Eng. 39, 3391–3403.

Peerlings, R., de Borst, R., Brekelmans, W., de Vree, J., Spee, I., 1996b. Some observations on localisation in non-local and gradient damage models. Eur. J. Mech. A/Solids 15, 937–953.

Petera, J., Pittman, J., 1994. Isoparametric hermite elements. Int. J. Numer. Methods Eng. 37, 3489–3519.

Pichugin, A., Askes, H., Tyas, A., 2008. Asymptotic equivalence of homogenisation procedures and fine-tuning of continuum theories. J. Sound Vibr. 313, 858–874.

Polizzotto, C., 2003. Gradient elasticity and nonstandard boundary conditions. Int. J. Solids Struct. 40, 7399–7423.

Polyzos, D., Tsepoura, K., Tsinopoulos, S., Beskos, D., 2003. A boundary element method of solving 2-D and 3-D static gradient elastic problems Part I: Integral formulation. Comput. Methods Appl. Mech. Eng. 192, 2845–2873.

Polyzos, D., Tsepoura, K., Beskos, D., 2005. Transient dynamic analysis of 3-D gradient elastic solids by BEM. Comput. Struct. 83, 783–792.

Price, D., Rowe, J., Nicklow, R., 1971. Lattice dynamics of grey tin and indium antomonide. Phys. Rev. B 3, 1268–1279.

Rajagopal, K., 2003. On implicit constitutive theories. Appl. Math. 48, 279–319.

Rajagopal, K., 2007. The elasticity of elasticity. Zeitsch. Angew. Math. Phys. 58, 309–317.

Rodríguez-Ferran, A., Morata, I., Huerta, A., 2005. A new damage model based on non-local displacements. Int. J. Numer. Analytical Methods Geom. 29, 473–493.

Ru, C., Aifantis, E., 1993. A simple approach to solve boundary-value problems in gradient elasticity. Acta Mech. 101, 59–68.

Rubin, M., Rosenau, P., Gottlieb, O., 1995. Continuum model of dispersion caused by an inherent material characteristic length. J. Appl. Phys. 77, 4054–4063.

Sansour, C., Skatulla, S., 2009. A strain gradient generalized continuum approach for modelling elastic scale effects. Comput. Methods Appl. Mech. Eng. 198, 1401–1412.

Savin, G., Lukashev, A., Lysko, E., 1970. Elastic wave propagation in a solid with microstructure. Int. Appl. Mech. 6, 725–728.

Shu, J., King, W., Fleck, N., 1999. Finite elements for materials with strain gradient effects. Int. J. Numer. Methods Eng. 44, 373–391.

Soh, A.-K., Wanji, C., 2004. Finite element formulations of strain gradient theory for microstructures and the C^{0-1} patch test. Int. J. Numer. Methods Eng. 61, 433–454.

Stavropoulou, M., Exadaktylos, G., Papamichos, E., Larsen, I., Ringstad, C., 2003. Rayleigh wave propagation in intact and damaged geomaterials. Int. J. Rock Mech. Mining Sci. 40, 377–387.

Suiker, A., de Borst, R., 2001. Micro-mechanical modelling of granular material. Part 1: derivation of a second-gradient micro-polar constitutive theory. Acta Mech. 149, 161–180. C.S.C..

Tang, Z., Shen, S., Atluri, S., 2003. Analysis of materials with strain-gradient effects: a Meshless Local Petrov Galerkin (MLPG) approach, with nodel displacements only. Comput. Model. Eng. Sci. 4, 177–196.

Tekoglu, C., Onck, P., 2005. Size effects in the mechanical behavior of cellular materials. J. Mater. Sci. 40, 5911–5917.

Tenek, L., Aifantis, E., 2002. A two-dimensional finite element implementation of a special form of gradient elasticity. Comput. Model. Eng. Sci. 3, 731–741.

Tomita, Y., Fujimoto, T., 1995. Plane-strain flow localization in tension blocks obeying strain-gradient-dependent constitutive equation. Mater. Sci. Res. Int. 1, 254–259.

Toupin, R., 1962. Elastic materials with couple-stresses. Arch. Rat. Mech. Anal. 11, 385–414.
Toupin, R., 1964. Theories of elasticity with couple-stress. Arch. Rat. Mech. Anal. 17, 85–112.
Triantafyllidis, N., Aifantis, E., 1986. A gradient approach to localization of deformation. I. Hyperelastic materials. J. Elast. 16, 225–237.
Tsepoura, K., Papargyi-Beskou, S., Polyzos, D., 2002. A boundary element method for solving 3D static gradient elastic problems with surface energy. Comput. Mech. 29, 361–381.
Tsepoura, K., Tsinopoulos, S., Polyzos, D., Beskos, D., 2003. A boundary element method of solving 2-D and 3-D static gradient elastic problems Part II: numerical implementation. Comput. Methods Appl. Mech. Eng. 192, 2875–2907.
Unger, D., Aifantis, E., 1995. The asymptotic solution of gradient elasticity for mode-III. Int. J. Fract. 71, R27–R32.
Unger, D., Aifantis, E., 2000a. Strain gradient elasticity theory for antiplane shear cracks. Part I: oscillatory displacements. Theor. Appl. Fract. Mech. 34, 243–252.
Unger, D., Aifantis, E., 2000b. Strain gradient elasticity theory for antiplane shear cracks. Part II: monotonic displacements. Theor. Appl. Fract. Mech. 34, 253–265.
Vardoulakis, I., Exadaktylos, G., Aifantis, E., 1996. Gradient elasticity with surface energy: mode-III crack problem. Int. J. Solids Struct. 33, 4531–4559.
Vasiliev, A., Dmitriev, S., Miroshnichenko, A., 2010. Multi-field approach in mechanics of structural solids. Int. J. Solids Struct. 47, 510–525.
Vdovin, V., Kunin, I., 1966. A theory of elasticity with spatial distribution of matter. Three-dimensional complex structure. J. Appl. Math. Mech. 30, 1272–1281.
Verble, J., Warren, J., Yarnell, J., 1968. Lattice dynamics of lithium hydride. Phys. Rev. 168, 980–989.
Voigt, W., 1887a. Theoretische Studien über die Elasticitätsverhältnisse der Krystalle. I. Ableitung der Grundgleichungen aus der Annahme mit Polarität begabter Moleküle. Abhandlungen der Mathematischen Classe der Königlichen Gesellschaft der Wissenschaften zu Göttingen 34, 3–52.
Voigt, W., 1887b. Theoretische Studien über die Elasticitätsverhältnisse der Krystalle. II. Untersuchung des elastischen Verhaltens eines Cylinders aus krystallinscher Substanz, auf dessen Mantelfläche keine Kräfte wirken, wenn die in seinem Innern wirkenden Spannungen längs der Cylinderaxe constant sind. Abhandlungen der Mathematischen Classe der Königlichen Gesellschaft der Wissenschaften zu Göttingen 34, 53–79.
Voigt, W., 1887c. Theoretische Studien über die Elasticitätsverhältnisse der Krystalle. III. Untersuchung des elastischen Verhaltens eines Cylinders aus krystallinscher Substanz, auf dessen Mantelfläche keine äussern Drucke wirken, wenn die in seinem Innern wirkenden Spannungen lineäre Functionen der Axenrichtung sind. Abhandlungen der Mathematischen Classe der Königlichen Gesellschaft der Wissenschaften zu Göttingen 34, 80–100.
Wang, L., Hu, H., 2005. Flexural wave propagation in single-walled carbon nanotubes. Phys. Rev. B 71, 195412.
Wang, L., Guo, W., Hu, H., 2008. Group velocity of wave propagation in carbon nanotubes. Proc. Roy. Soc. A 464, 1423–1438.
Warren, J., Yarnell, J., Dolling, G., Cowley, R., 1967. Lattice dynamics of diamond. Phys. Rev. 158, 805–808.
Yang, J., Guo, S., 2005. On using strain gradient theories in the analysis of cracks. Int. J. Fract. 133, L19–L22.
Yarnell, J., Warren, J., Wenzel, R., 1964a. Lattice vibrations in diamond. Phys. Rev. Lett. 13, 13–15.
Yarnell, J., Warren, J., Wenzel, R., Koenig, S., 1964b. Phonon dispersion curves in bismuth. IBM J. Res. Dev. 8, 234–240.
Zervos, A., 2008. Finite elements for elasticity with microstructure and gradient elasticity. Int. J. Numer. Methods Eng. 73, 564–595.
Zervos, A., Papanastasiou, P., Vardoulakis, I., 2001. A finite element displacement formulation for gradient elastoplasticity. Int. J. Numer. Methods Eng. 50, 1369–1388.
Zervos, A., Papanicolopulos, S.-A., Vardoulakis, I., 2009. Two finite element discretizations for gradient elasticity. ASCE J. Eng. Mech. 135, 203–213.